

Introducing Decorated HODs: modeling assembly bias in the galaxy-halo connection

Andrew P. Hearin¹, Andrew R. Zentner², Frank C. van den Bosch³,
Duncan Campbell³, Erik Tollerud^{3,4}

¹Yale Center for Astronomy & Astrophysics, Yale University, New Haven, CT

²Department of Physics and Astronomy & Pittsburgh Particle Physics, Astrophysics, and Cosmology Center (PITT PACC), University of Pittsburgh, Pittsburgh, PA 15260

³Department of Astronomy, Yale University, P.O. Box 208101, New Haven, CT

⁴Space Telescope Science Institute, 3700 San Martin Dr, Baltimore, MD 21218

6 March 2022

ABSTRACT

The connection between galaxies and dark matter halos is often inferred from data using probabilistic models, such as the Halo Occupation Distribution (HOD). Conventional HOD formulations assume that *only* halo mass governs the galaxy-halo connection. Violations of this assumption, known as *galaxy assembly bias*, threaten the HOD program. We introduce *decorated HODs*, a new, flexible class of models designed to account for assembly bias. Decorated HODs minimally expand the parameter space and maximize the independence between traditional and novel HOD parameters. We use decorated HODs to quantify the influence of assembly bias on clustering and lensing statistics. For SDSS-like samples, the impact of assembly bias on galaxy clustering can be as large as a factor of two on $r \sim 200$ kpc scales and $\sim 15\%$ in the linear regime. Assembly bias can either enhance or diminish clustering on large scales, but generally increases clustering on scales $r \lesssim 1$ Mpc. We performed our calculations with **Halotools**, an open-source, community-driven python package for studying the galaxy-halo connection (<http://halotools.readthedocs.org>). We conclude by describing the use of decorated HODs to treat assembly bias in otherwise conventional likelihood analyses.

Key words: cosmology: theory — dark matter — galaxies: halos — galaxies: evolution — galaxies: clustering — large-scale structure of universe

1 INTRODUCTION

The last decade has seen the development of a new, powerful technique to inform models of galaxy formation, interpret large-scale structure, and constrain cosmological parameters. This technique, called halo occupation modeling, establishes a statistical connection between galaxies and dark matter halos. Using clustering and lensing data from various galaxy redshift surveys, halo occupation modeling has been used to put tight constraints on the stellar mass-to-halo mass relation of galaxies from redshift $z = 0$ to $z \sim 2$ (Yang et al. 2003; Tinker et al. 2005; van den Bosch et al. 2007; Zheng et al. 2007; Wake et al. 2011; Leauthaud et al. 2012), which in turn has put tight constraints on the co-evolution of galaxies and their host halos across cosmic time (Conroy & Wechsler 2009; Yang et al. 2009b, 2011, 2012; Behroozi et al. 2013; Moster

et al. 2013). In addition, this technique is routinely used to infer the masses of dark matter halos that host extreme populations, such as quasars (Porciani et al. 2004; Porciani & Norberg 2006), Lyman-break galaxies (Bullock et al. 2001), or luminous red galaxies (Wake et al. 2008), while applications to star forming and quenched galaxies separately has proven instrumental for learning about the demographics of galaxy quenching (van den Bosch et al. 2003; Zehavi et al. 2005, 2011; Collister & Lahav 2005; Skibba & Sheth 2009; Rodriguez-Puebla et al. 2011; Tinker et al. 2013; Guo et al. 2011, 2014; Zu & Mandelbaum 2015). And finally, halo occupation modeling is used to test cosmology on small scales (e.g., van den Bosch et al. 2003; Tinker et al. 2005; Cacciato et al. 2013; More et al. 2013).

The key concept that underlies halo occupation modeling is that all galaxies reside in dark matter halos, and

that these halos themselves are biased tracers of the dark matter density field. If the so-called “halo bias” b_h were only a function of halo mass, then knowledge of the manner by which galaxies reside in halos as a function of halo mass would be sufficient to make predictions for the large-scale galaxy clustering that we observe.

However, it is now well-established that halo clustering depends upon attributes other than halo mass, including halo formation time and concentration (e.g., Gao et al. 2005; Wechsler et al. 2006; Gao & White 2007; Zentner 2007; Dalal et al. 2008; Lacerna & Padilla 2011). Such dependence of the spatial distribution of dark matter halos upon properties besides mass is generically referred to as *halo assembly bias*, and on large scales it can be quantified as $b_h = b_h(M, X)$, where X is the set of halo properties other than halo mass that influence halo bias. If the relationship between galaxies and halos depends upon any of these additional halo properties X , then conventional occupation models will fail.

Despite this threat of assembly bias, virtually all studies of halo occupation statistics published to date are predicated upon the assumption that the mass of a dark matter halo, M_h , *completely* determines the statistical properties of its resident galaxy population.¹ Under this ‘Mass-Only ansatz’, the properties of galaxies that reside in halos of fixed mass are uncorrelated with any other halo property, and *any* environmental dependence of galaxies is merely a manifestation of different environments probing different halo masses.

In light of our standard paradigm for galaxy formation (see Mo et al. 2010, for an overview and extensive list of references), in which galaxy growth is governed by halo growth, galaxy size is linked to halo spin, galaxy morphology is related to halo merger history, and star formation quenching is triggered by local environmental processes, such an ansatz is suspect. Indeed, semi-analytical models for galaxy formation predict significant correlations between galaxy properties and halo properties other than mass (e.g., Zhu et al. 2006; Croton et al. 2007); such correlations are also present in hydrodynamical simulations of galaxy formation and evolution (Feldmann & Mayer 2015; Bray et al. 2016).

The Mass-Only ansatz was not proposed with any theoretical prejudice regarding galaxy formation; rather, it is the simplest implementation that has proven to be successful in fitting the clustering properties of the available data. Consequently, it is generally argued that the impact of assembly bias, if present, is too weak to have a significant impact, and that there is thus no need for more sophisticated models (e.g., Tinker et al. 2008). This argument is strengthened by several studies that have demonstrated that halo mass is clearly the dominant parameter governing the environmental demographics of galaxies (e.g., Mo et al. 2004; Kauffmann et al. 2004; Blanton et al. 2006).

Zentner et al. (2014) demonstrated explicitly that ig-

oring assembly bias in halo occupation modeling yields constraints on the galaxy-dark matter connection that may be plagued by significant, systematic errors. The magnitude of this error is especially large for extreme populations, such as star forming or quenched galaxies, and calls into question many of the inferences that have been made using halo occupation modeling. Furthermore, some level of galaxy assembly bias seems difficult to avoid, given that the abundance of subhalos (which is directly related to the occupation number of satellite galaxies) depends strongly on the assembly time of the host halo (Zentner et al. 2005; van den Bosch et al. 2005; Mao et al. 2015; Jiang & van den Bosch 2015); hence, one expects that earlier-forming, more strongly-clustered host halos have fewer satellite galaxies.

Additionally, a number of studies have presented compelling evidence that observational data is affected by galaxy assembly bias. Yang et al. (2006) showed that, at fixed halo mass, the clustering strength increases as the star formation rate of the central galaxy decreases (see also Wang et al. 2008, 2013; Lin et al. 2015). In Blanton & Berlind (2007) it was shown that shuffling the colors and luminosities of galaxies among groups of similar mass modifies the clustering at the $\sim 5 - 10\%$ level. More recently, Miyatake et al. (2015) reported a strong detection of assembly bias in an SDSS sample of galaxy clusters. Another manifestation of assembly bias was presented by Weinmann et al. (2006), who showed that, at fixed group (halo) mass, both the color and star formation rate (SFR) of satellite galaxies depend on the color/SFR of the group’s central galaxy. Kauffmann et al. (2013) demonstrated that this ‘galactic conformity’ (i.e., spatial correlations in specific star formation rates) persists out to several Mpc. As emphasized in Hearin et al. (2014), if halo mass has been properly controlled for in the observational measurements, then conformity manifestly violates the Mass-Only ansatz, and is a smoking-gun signature of galaxy assembly bias.

To summarize, without some remedy for assembly bias, halo occupation modeling is doomed to hit a systematic error “ceiling” before realizing its potential to exploit the wealth of extant and forthcoming observational data in an optimal and unbiased way. To address this challenge, in this paper we introduce a natural extension of the standard Halo Occupation Distribution (HOD) formalism with parametric freedom that allows for galaxy assembly bias. This *decorated HOD* describes the halo occupation statistics in terms of two halo properties rather than one. In this pilot study we describe the formalism and demonstrate how the extra degree of freedom can cause dramatic changes in the clustering and lensing of galaxies, further advocating a proper treatment of assembly bias.

All calculations in this paper are performed using *Halotools*, a new open-source, community-driven python package for studying the galaxy-halo connection (<http://halotools.readthedocs.org>). *Halotools* is built upon the Astropy package-template² and is being developed to be an Astropy-affiliated package

¹ Some models replace halo mass by a single other halo property, such as the maximum circular velocity of the halo. The upshot remains the same; it is implicitly assumed that the occupation statistics depend on that property alone.

² See <https://github.com/astropy/package-template>.

(Astropy Collaboration et al. 2013).³ Since its inception, *Halotools* has been developed in public on <https://github.com/astropy/halotools>, in the spirit of open science.

The remainder of this paper is organized as follows. We give a pedagogical review of standard halo occupation methods in §2. In §3 we describe how we use the *Halotools* package to conduct all of our halo-occupation and large-scale structure calculations. We develop the analytical formalism of the decorated HOD in §4. In §5 we use a simple implementation of the decorated HOD to estimate the magnitude and scale-dependence of the effects galaxy assembly bias can have on galaxy clustering and galaxy-galaxy lensing. We conclude in §6 by comparing our model to previous formulations of the galaxy-halo connection, and by describing the significance of our results for the precision cosmology program. We summarize our primary findings in §7.

2 STANDARD HOD MODEL

In halo models of the galaxy distribution, it is assumed that every galaxy resides in some dark matter halo. Under this assumption, knowledge of how galaxies populate, and are distributed within, dark matter halos is sufficient to describe the statistics of the observed galaxy distribution (e.g. Seljak 2000; Ma & Fry 2000; Scoccimarro et al. 2001; Berlind & Weinberg 2002). In this section, we discuss the standard halo models of galaxy clustering with an eye toward pedagogy in order to enable qualitative understanding of results that follow later in the paper.

2.1 HOD formulation of Galaxy Clustering

One of the most well-studied statistics of the galaxy distribution is the galaxy-galaxy correlation function, $\xi_{gg}(r)$, which expresses the probability in excess of random of finding a pair of galaxies separated by three-dimensional distance r . By dividing galaxy pair-counts into terms containing either pairs residing in the same dark matter halo or pairs of galaxies residing in distinct halos, ξ_{gg} can be decomposed into a “one-halo term” and a “two-halo term”,

$$\xi_{gg}(r) = 1 + \xi_{gg}^{1h}(r) + \xi_{gg}^{2h}(r).$$

As mentioned briefly in the introduction, one of the leading approaches to characterizing the galaxy-halo connection is via the Halo Occupation Distribution (HOD). In the HOD approach, the central quantity is $P(N_g|M_h)$, the probability that a halo of mass M_h hosts N_g galaxies. Given a specific HOD, the one- and two-halo terms of the galaxy correlation function can be computed in terms of the first two moments of $P(N_g|M_h)$:

$$1 + \xi_{gg}^{1h}(r) \simeq \frac{1}{4\pi r^2 \bar{n}_g^2} \int dM_h \frac{dn}{dM_h} \Xi_{gg}(r|M_h) \times \langle N_g(N_g - 1) | M_h \rangle, \quad (1)$$

³ See <http://www.astropy.org/affiliated>.

and

$$\xi_{gg}^{2h}(r) \simeq \xi_{mm}(r) \times \left[\frac{1}{\bar{n}_g} \int dM_h \frac{dn}{dM_h} \langle N_g | M_h \rangle b_h(M_h) \right]^2 \quad (2)$$

In Eqs. (1) and (2), \bar{n}_g is the cosmic mean number density of the galaxy sample, dn/dM_h is the halo mass function, $b_h(M_h)$ the spatial bias of dark matter halos, and ξ_{mm} is the dark matter two-point correlation function. If the spatial distribution of galaxies within a halo is represented by a spherically symmetric, unit-normalized number density $n_g(r)$, then the quantity $\Xi_{gg}(r)$ is the convolution of $n_g(r)$ with itself. Note that we have employed several simplifying assumptions in these expressions for the correlation function; in particular, halos and their associated galaxy distributions are assumed to be spherically symmetric, the halo bias is assumed to have no radial dependence, and halo exclusion is not taken into account (see e.g., Cooray & Sheth 2002; Mo et al. 2010; van den Bosch et al. 2013, and references therein). As we describe in §3, the *Halotools* methodology used in the present work has the distinct advantage that it is immune to errors and uncertainties arising from these approximations.

Under the same simplifying assumptions as above, one can use the same formalism to also express the one- and two-halo terms of the galaxy-matter cross-correlation function, ξ_{gm} , as

$$1 + \xi_{gm}^{1h} \simeq \frac{1}{4\pi r^2 \bar{n}_g \bar{\rho}_m} \int dM_h \frac{dn}{dM_{\text{vir}}} \Xi_{gm}(r|M_h) \times \langle N_g | M_h \rangle, \quad (3)$$

and

$$\xi_{gm}^{2h} \simeq \xi_{mm}(r) \times \left[\frac{1}{\bar{n}_g} \int dM_h \frac{dn}{dM_h} \langle N_g | M_h \rangle b_h(M_h) \right] \times \left[\frac{1}{\bar{\rho}_m} \int dM_h \frac{dn}{dM_h} b_h(M_h) \right] \quad (4)$$

Here, $\bar{\rho}_m$ is the mean matter density in the universe, and Ξ_{gm} is the convolution of the normalized dark matter halo density profile with $n_g(r)$. Note that ξ_{gm} is the fundamental two-point function underlying the excess surface densities probed by the galaxy-galaxy lensing signal (e.g., Mandelbaum et al. 2005; Seljak et al. 2005; Yoo et al. 2006; Cacciato et al. 2009).

2.2 Central-Satellite Decomposition

Conventionally, occupation statistics of central galaxies are modeled separately from satellites, so that $\langle N_g | M_h \rangle = \langle N_c | M_h \rangle + \langle N_s | M_h \rangle$. The starting point for any HOD-style model is then choosing an analytical form for $\langle N_c \rangle$ and $\langle N_s \rangle$. Central galaxies are commonly assumed to reside at the center of the halo, so that $n_{\text{cen}}(r) = \delta(r)$, while satellite galaxies are typically assumed to follow a radial number density distribution, $n_{\text{sat}}(r)$, that traces the NFW density distribution (Navarro et al. 1997) of the underlying dark matter halo, albeit with a concentration

parameter that is sometimes allowed to differ from that of the dark matter.

Consider Eq. (1) in light of this decomposition. The one-halo term receives a contribution from the second satellite moment, $\langle N_s(N_s - 1)|M_h \rangle$; computing this contribution requires additional assumptions beyond a model for $\langle N_s|M_h \rangle$. Motivated by the occupation statistics of subhalos in high-resolution N-body simulations (Kravtsov et al. 2004), the PDF of satellite occupation is commonly assumed to be Poissonian, so that $\langle N_s(N_s - 1)|M_h \rangle = \langle N_s|M_h \rangle^2$.

2.3 Central-Satellite Correlations

The one-halo term in Eq. (1) also contains a contribution from $\langle N_c N_s|M_h \rangle$, which itself requires an additional assumption to compute. In the vast majority of HOD studies, it is assumed that the satellite and central HODs are completely uncorrelated; however, we are unaware of any data indicating that this should be the case despite theoretical prejudices that N_c and N_s may well be correlated. If satellites have no knowledge of the central galaxy occupation of their host halos, then $\langle N_c N_s|M_h \rangle = \langle N_c|M_h \rangle \langle N_s|M_h \rangle$. On the other hand, if the presence of a central in a halo is required for one or more satellites to occupy that halo, then $\langle N_c N_s|M_h \rangle = \langle N_s|M_h \rangle$. It may also be possible that centrals and satellites “repel” each other so that they never reside in the same halo, in which case $\langle N_c N_s|M_h \rangle = 0$. These possibilities represent the extremes of no correlation, complete correlation, and complete anticorrelation. Galaxy samples selected from the observed universe likely exhibit correlations somewhere between these extremes.

The means by which $\langle N_c N_s|M_h \rangle$ is computed is not simply academic: both Reid et al. (2014) and Guo et al. (2014) have shown that the satellite fraction inferred from HOD analyses of BOSS galaxies is impacted at the $\sim 50\%$ level depending on whether one assumes maximal or zero central-satellite correlations (see also Ross & Brunner 2009, for analogous findings for color-selected samples). Zentner et al. (2014) demonstrated that identical HODs with distinct central-satellite correlations motivated by physical considerations can lead to large (as much as a factor of ~ 2), scale-dependent differences in correlation functions for separations $r \lesssim 1$ Mpc.

The degree of central-satellite correlation is more than simply a nuisance systematic. Such correlations are induced by astrophysics that is interesting in its own right and which we aim to learn about through the analysis of statistically-large galaxy samples. This correlation encodes the extent to which the properties of a satellite galaxy (stellar mass, color, etc.) may be correlated with the properties of its central galaxy at fixed halo mass. Such a correlation could easily arise, for example, from galactic cannibalism: if a satellite galaxy merges with the central galaxy, the latter’s mass increases while N_s decreases (e.g., Purcell et al. 2007); in addition, the one-halo galactic conformity detected by Weinmann et al. (2006) is an example of a correlation between central and satellite properties. As we will see, the decorated HOD formalism introduced in §4 naturally permits an analytical means to

explore parametrically cases of intermediary correlation between the two extremes sketched above, so that quantitative constraints can be placed on the effects giving rise to central-satellite correlations.

2.4 Baseline HOD Parameterization

In order to understand the potential influence of assembly bias, we perturb the galaxy-halo connection about a baseline HOD model that has no assembly bias. For the remainder of this paper, unless otherwise specified, we use the HOD parameterization introduced in Leauthaud et al. (2011) as our baseline model. In this model, the first occupation moment of central galaxies $\langle N_c|M_h \rangle$ is defined in terms of the conditional stellar mass function (CSMF), $\phi_c(M_*|M_h)$; the CSMF is the probability distribution for the stellar mass of a central galaxy residing in a halo of mass M_h (Yang et al. 2003, 2009a). For a volume-limited sample of galaxies more massive than M_*^{thresh} , the relationship between $\langle N_c \rangle$ and $\phi_c(M_*|M_h)$ is given by:

$$\langle N_c|M_h \rangle = \int_{M_*^{\text{thresh}}}^{\infty} dM_* \phi_c(M_*|M_h) \quad (5)$$

The function $\phi_c(M_*|M_h)$ is assumed to be a log-normal distribution with a first moment that varies with halo mass according to the stellar-to-halo-mass relation $\bar{M}_*(M_h)$. For $\bar{M}_*(M_h)$ we use the model developed in Behroozi et al. (2010), in which the stellar-to-halo-mass relation is defined by the inverse relation $\bar{M}_h(M_*)$,

$$\log_{10}[\bar{M}_h(M_*)] = \log_{10}(M_1) + \beta \log_{10}\left(\frac{M_*}{M_{*,0}}\right) + \frac{(M_*/M_{*,0})^\delta}{1 + (M_*/M_{*,0})^{-\gamma}} - \frac{1}{2}. \quad (6)$$

One can then compute the stellar-to-halo-mass relation $\bar{M}_*(M_h)$ by numerically inverting Eq. (6). The model for $\bar{M}_*(M_h)$ at redshift-zero therefore has five parameters: M_1 is the characteristic halo mass, $M_{*,0}$ is the characteristic stellar mass, β is the low-mass slope, δ the high-mass slope, and γ controls the transition region.

We will model redshift-dependence in the HOD by allowing the parameters of $\bar{M}_*(M_h)$ to vary linearly with the scale factor, as in Behroozi et al. (2010), so that

$$\begin{aligned} M_{*,0}(a) &= M_{*,0} - (1-a)M_{*,a} \\ M_1(a) &= M_1 - (1-a)M_{1,a} \\ \beta(a) &= \beta - (1-a)\beta_a \\ \gamma(a) &= \gamma - (1-a)\gamma_a \\ \delta(a) &= \delta - (1-a)\delta_a \end{aligned} \quad (7)$$

The model for $\bar{M}_*(M_h, z)$ across redshift then has a total of $5 \times 2 = 10$ parameters. Throughout this paper, the values of all ten of these parameters are taken directly from column 1 of Table 2 of Behroozi et al. (2010).

Throughout this paper, we assume that $\phi_c(M_*|M_h)$ has constant scatter $\sigma_{\log M_*}$, which will serve as the 11th parameter governing central occupations statistics across redshift. Under the log-normal assumption the first occupation moment of central galaxies can be computed

analytically as:

$$\langle N_c | M_h \rangle = \frac{1}{2} - \frac{1}{2} \operatorname{erf} \left(\frac{\log_{10}(M_*^{\text{thresh}}) - \log_{10}[\bar{M}_*(M_h)]}{\sqrt{2}\sigma_{\log M_*}} \right). \quad (8)$$

We will explicitly study how the impact of assembly bias is influenced by the level of scatter, but unless otherwise stated we will use $\sigma_{\log M_*} = 0.4$ as our fiducial value.

The first occupation moment of satellites is modeled as

$$\langle N_s | M_h \rangle = \langle N_c | M_h \rangle (M_h / M_{\text{sat}})^{\alpha_{\text{sat}}} e^{-M_{\text{cut}} / M_h}. \quad (9)$$

The parameter α_{sat} controls the power-law increase in satellite number with halo mass; M_{sat} defines the amplitude of the power law; and M_{cut} sets the scale of an exponential cutoff that guarantees that halos with masses $M_h \ll M_{\text{cut}}$ are extremely unlikely to host a satellite galaxy. In light of the discussion in §2.2, note that $\langle N_s | M_h \rangle$ depends on $\langle N_c | M_h \rangle$, indicating that in this particular model the occupation statistics of centrals and satellites are correlated. The satellite amplitude is parameterized as

$$M_{\text{sat}} = 10^{12} M_{\odot} B_{\text{sat}} \left[\frac{\bar{M}_h(M_*^{\text{thresh}})}{10^{12} M_{\odot}} \right]^{\beta_{\text{sat}}}, \quad (10)$$

while the cutoff is parameterized as

$$M_{\text{cut}} = 10^{12} M_{\odot} B_{\text{cut}} \left[\frac{\bar{M}_h(M_*^{\text{thresh}})}{10^{12} M_{\odot}} \right]^{\beta_{\text{cut}}}. \quad (11)$$

Satellite occupation statistics therefore have five parameters, namely α_{sat} , B_{sat} , β_{sat} , B_{cut} and β_{cut} . We set the values of these parameters in our fiducial baseline model to be those listed in the “SIG_MOD1” values of Table 5 in Leauthaud et al. (2012), to which we refer the reader for a full discussion of this model.

By using this model, we are working with an HOD parameterization that has been used to describe survey data with success. This model has sufficient complexity to be relevant to the interpretation of observations. This adds to the realism and relevance of the calculations that follow. However, we should note that if assembly bias is a non-negligible effect in the universe, these HODs may be systematically in error (e.g., Zentner et al. 2014) and we may not be perturbing about the true, underlying, mass-only baseline HOD realized in nature.

3 HALO OCCUPATION MODELING WITH HALOTOOLS

The conventional analytical methods for calculating ξ_{gg} and ξ_{gm} described in §2 rely on a large number of assumptions and restrictions that limit the accuracy of these commonly-used techniques. Halos are typically assumed to be spherical, virialized matter distributions, characterized by an NFW profile (Navarro et al. 1997), while fitting functions for the halo mass function dn/dM_h and large-scale halo bias $b_h(M_h)$ are only accurate to the $\sim 5\%$ level (Tinker et al. 2008, 2010). In addition, halo exclusion and scale-dependence of the halo bias are difficult to treat properly, resulting in additional uncertainties and

inaccuracies (van den Bosch et al. 2013). Details regarding the implementations of these assumptions vary from author to author, and can give rise to systematic uncertainties that easily exceed 10%. Hence, if the demands for sub-percent accuracy of the precision-cosmology program are to be taken seriously, it is clear that conventional analytical methods face a serious problem.

The **Halotools** package is designed to remedy these and other shortcomings of conventional large-scale structure analyses by directly populating dark matter halos in numerical simulations with mock galaxies. **Halotools** therefore makes no appeal whatsoever to fitting functions for the abundance or spatial distribution of dark matter halos, while automatically taking halo exclusion into account. In addition, large-scale structure observables such as clustering and lensing are computed in **Halotools** directly from the mock galaxy distributions, using exactly the same method as used for the actual observational measurements. Finally, we stress that all calculations have been heavily optimized for MCMC-type applications.

Written exclusively in Python,⁴ **Halotools** provides a highly modular, object-oriented platform for building halo occupation models, so that individual modeling features can easily be swapped in and out. Beyond the conveniences of readability and ease-of-development that comes with using contemporary design patterns in a modern programming language, this modularity facilitates rigorous, systematic study of each and every component that makes up a halo occupation model. Of particular relevance to the present work is that **Halotools** has been designed from the ground-up with assembly bias applications in mind.

Ultimately, in order for any cosmological likelihood analysis to proceed it will be necessary to calibrate new fitting functions or emulators (e.g., Heitmann et al. 2009, 2010) so that predictions can be made for un-simulated sets of cosmological parameters. Either **Halotools**, or a package very much like it, will need to go hand-in-hand with such an effort, as direct-mock-population provides the gold standard of precision for large-scale structure predictions.

Although the equations in §2 are indeed only rough approximations, these equations are and will remain useful to gain physical insight into the connection between occupation statistics and two-point clustering. Throughout the paper, however, for all our results concerning galaxy clustering and lensing, we do not perform our calculations using Eqs. (1)-(4). Instead, we calculate ξ_{gg} and ξ_{gm} by using **Halotools** to populate dark matter halos with mock galaxies and then apply the Landy & Szalay (1993) estimator on the resulting set of point data. In §3.1 we provide a brief sketch of the Monte Carlo techniques used in this mock population; we refer the reader to <http://halotools.readthedocs.org> for comprehensive documentation of these methods. We describe the simulation and halo catalogs we use in §3.2.

⁴ Some specific performance-critical elements are implemented with Cython (Behnel et al. 2011), a tool that compiles a python-like code into C code (<http://cython.org>).

3.1 Monte Carlo Methods

To populate halos with central galaxies, first we calculate the value of $\langle N_c \rangle$ for every halo in the simulation. For standard HOD models we use Eq. (8), whereas for assembly-biased models we use the analytical expressions derived in §4 below. For every halo in the simulation, we then draw a random number r from $\mathcal{U}(0, 1)$, a uniform distribution between zero and unity; for all halos with $r \leq \langle N_c \rangle$, we place a central galaxy at the halo center, leaving all other halos devoid of centrals.

Populating satellites is more complicated because the spatial distributions are non-trivial. The first step is the same: we compute $\langle N_s \rangle$ for every halo, using either Eq. (9) or the methods of §4, whichever is appropriate for the model in question. For each halo, we then determine the number of satellites that will be assigned to the halo by drawing an integer from the assumed satellite occupation distribution, $P(N_s|M_h)$ (or $P(N_s|M_h, x)$, see §4).

In this paper, we use the **Halotools** framework to model satellites as being isotropically distributed within their halos according to a NFW profile with concentration given by the value in the halo catalog.⁵ We generate Monte Carlo realizations of both radial and angular positions via the method of inverse transformation sampling, which we sketch in the following paragraph. Briefly, first we generate realizations of points uniformly distributed on the unit sphere; we then multiply these halo-centric x, y, z coordinates by the corresponding realization of the radial position.

To realize points on the unit sphere, we draw random numbers ϕ and $t \equiv \cos(\theta)$ from $\mathcal{U}(0, 1)$, computing $\sin(\theta) = \sqrt{1 - t^2}$. The x, y, z positions on the unit sphere are then computed as $x = \sin(\theta) \cos(\phi)$, $y = \sin(\theta) \sin(\phi)$, and $z = \cos(\theta)$. For the radial positions, first we calculate $P_{\text{NFW}}(< \tilde{r}|c)$, the cumulative probability function of the mass profile of an NFW halo with concentration c :

$$P_{\text{NFW}}(< \tilde{r}|c) \equiv \frac{M_{\text{NFW}}(< \tilde{r}|c)}{M_{\text{tot}}} = \frac{g(c\tilde{r})}{g(c)}, \quad (12)$$

where $g(x) \equiv \ln(1+x) - \frac{x}{1+x}$, and $\tilde{r} \equiv r/R_{\text{vir}}$. For a halo with concentration c populated by N_s satellites, we draw N_s random numbers p from $\mathcal{U}(0, 1)$. Each value p is interpreted as a probability where the corresponding value for the scaled radius \tilde{r} comes from numerically inverting $p = P_{\text{NFW}}(< \tilde{r}|c)$. Scaling the x, y, z points on the unit sphere by the value r gives the halo-centric position of the satellites.

3.2 Simulation and Halo Catalogs

Throughout this paper, the foundation of our results is the collisionless N-body Bolshoi simulation (Klypin et al. 2011). The Λ CDM cosmological parameters of Bolshoi are $\Omega_m = 0.27$, $\Omega_\Lambda = 0.73$, $\Omega_b = 0.042$, $n_s = 0.95$, $\sigma_8 = 0.82$, and $H_0 = 70 \text{ km s}^{-1} \text{ Mpc}^{-1}$. The gravity-solver of the simulation is the Adaptive Refinement Tree

⁵ The modular design of **Halotools** of course permits alternative modeling choices for the intra-halo distribution, e.g., simulated subhalo positions can be used directly.

code (ART; Kravtsov et al. 1997; Gottloeber & Klypin 2008), run on 2048³ particles in a 250Mpc periodic box. Bolshoi particles have a mass of $m_p \approx 1.35 \times 10^8 M_\odot$; the force resolution of the simulation is $\epsilon \approx 1 \text{ kpc}$. Here and throughout the paper, all numerical values of length and mass will be understood to be in $h = 1$ units. Snapshot data and halo catalogs for Bolshoi are part of the Multidark Database (Riebe et al. 2011), accessible at <http://www.multidark.org>.

We use the **ROCKSTAR** halo finder (Behroozi et al. 2011, 2013) to identify host halos in the $z = 0$ Bolshoi snapshot. Halo catalogs based on **ROCKSTAR** are publicly available at <http://hipacc.ucsc.edu/Bolshoi/MergerTrees.html>. Halos in these catalogs are defined to be spherical regions centered on a local density peak, such that the average density inside the sphere is $\Delta_{\text{vir}} \approx 360$ times the mean matter density of the simulation box. The radius of each such sphere defines the virial radius R_{vir} of the halo; the mass enclosed inside this sphere is the so-called “virial mass” $M_{\text{vir}} = \frac{4}{3}\pi R_{\text{vir}}^3 \Delta_{\text{vir}} \Omega_m \rho_{\text{crit}}$, where $\rho_{\text{crit}} = 3H_0^2/8\pi G$ is the critical energy density of the universe. In the model developed in this work, it will be useful to refer to a more generic halo mass M_h that is defined according to some density threshold that may deviate from Δ_{vir} , but it will be understood that all our numerical computations were carried out on halos defined according to Δ_{vir} .

4 GENERALIZING THE HOD

4.1 Basic Considerations

The standard HOD formalism described in §2 presumes that halo mass is the sole property that influences the probability that a (host) dark matter halo contains one or more galaxies in some sample. If there exists some halo property x , such that the HOD depends upon both x and M_h , $P(N_g|M_h, x) \neq P(N_g|M_h)$, and the clustering of halos depends upon x , then the dependence of the HOD on x must be accounted for in order to faithfully model the clustering of galaxies. *Galaxy assembly bias* refers to the situation when there exists such a property x .

In this section, we discuss a simple and convenient generalization of the HOD formalism to account for galaxy assembly bias. The formalism that we describe is general in the sense that it can, in principle, be applied to any halo property in addition to halo mass and it can be straightforwardly extended to describe HODs that depend upon numerous additional halo properties.

4.1.1 The principle of HOD conservation

We will differentiate between the occupation statistics of a standard HOD model and a *decorated* HOD model by denoting these two distributions as P_{std} and P_{dec} , respectively, so that

$$P_{\text{std}}(N_g|M_h, x) = P_{\text{std}}(N_g|M_h),$$

but

$$P_{\text{dec}}(N_g|M_h, x) \neq P_{\text{dec}}(N_g|M_h).$$

In the decorated HOD, we will refer to the *conditional moments of order k* as

$$\langle N_g^k | M_h, x \rangle_{\text{dec}} \equiv \sum_{N_g=0}^{\infty} N_g^k P_{\text{dec}}(N_g | M_h, x), \quad (13)$$

and the corresponding *marginalized moments* as

$$\langle N_g^k | M_h \rangle_{\text{dec}} \equiv \int \langle N_g^k | M_h, x \rangle_{\text{dec}} P(x | M_h) dx, \quad (14)$$

where $P(x | M_h)$ is the normalized probability distribution that a halo of mass M_h has a particular value of x .

Beginning with any standard HOD, our goal is to identify the conditions under which the marginalized moments of a new, decorated model are equal to the moments of the standard model:

$$\langle N_g^k | M_h \rangle_{\text{dec}} = \langle N_g^k | M_h \rangle_{\text{std}}. \quad (15)$$

Eq. (15) defines our notion of *HOD conservation*; we will say that any model $P_{\text{dec}}(N_g | M_h, x)$ with marginalized moments that respect Eq. (15) *preserve the moments of $P_{\text{std}}(N_g | M_h)$* . Conserving the HOD minimizes the modifications that are needed to allow for assembly bias. By using decorated HODs that are modeled off of existing HODs one can continue to reap the benefits of the infrastructure that has been developed over the past decade.

Now we will define a perturbation to the halo occupation induced by the auxiliary variable x ,

$$\delta N_g^k(M_h, x) \equiv \langle N_g^k | M_h, x \rangle_{\text{dec}} - \langle N_g^k | M_h \rangle_{\text{std}}. \quad (16)$$

We will refer to δN_g^k as the k^{th} -order *decoration function*. The $\delta N_g^k(x, M_h)$ represent the change in the moments of the decorated HOD with respect to a standard HOD without assembly bias. Using this definition, Eq. (15) becomes

$$0 = \int \delta N_g^k(M_h, x) P(x | M_h) dx \quad (17)$$

for all $k = 1, 2, 3, \dots$. Whenever no confusion can arise, we will drop the superscript and it will be understood that $\delta N_g = \delta N_g^1$.

4.1.2 Application to centrals

Let us proceed by considering the central and satellite populations separately because different assumptions are typically made to describe these distributions. In particular, halos have either zero or one central galaxy and the HOD (both decorated and standard) therefore follows a nearest-integer distribution. This implies that

$$\langle N_g^k | M_h, x \rangle_{\text{dec}} = \langle N_g^1 | M_h, x \rangle_{\text{dec}} \quad (18)$$

for all k . Hence, once Eq. (15) is satisfied for $k = 1$, it is trivially satisfied for all higher-order central moments. Therefore, in order to construct decorated HOD models that preserve the full $P_{\text{std}}(N_c | M_h)$ we only need to ensure that the first-order decoration function δN_c^1 respects

$$0 = \int \delta N_c^1(M_h, x) P(x | M_h) dx.$$

4.1.3 Application to satellites

Moving on, consider the more difficult case of satellite galaxies. Typically, satellite galaxies are considered to be drawn from a Poisson distribution. We begin with the natural assumption that both $P_{\text{dec}}(N_s | M_h)$ and $P_{\text{dec}}(N_s | M_h, x)$ are Poisson distributions. Under this Poisson assumption, as well as the assumption that the first moment of the HOD is preserved, one can show that

$$0 = \int [\delta N_s^1(M_h, x)]^2 P(x | M_h) dx. \quad (19)$$

Eq. (19), however, cannot be satisfied for a non-trivial decoration function $\delta N_s^1(x)$ because the integrand is non-negative over its entire domain. *If we wish for both $P(N_s | M_h)$ and $P(N_s | M_h, x)$ to obey Poisson statistics then it is not possible to conserve the HOD.* The converse is also true: if we insist on conserving the HOD, one cannot have both $P(N_s | M_h)$ and $P(N_s | M_h, x)$ obey Poisson statistics.

There are numerous reasonable ways to proceed. First, one could assume that *both* $P_{\text{std}}(N_s | M_h)$ and $P_{\text{dec}}(N_s | M_h, x)$ are Poisson distributions. This implies that

$$\langle N_s(N_s - 1) | M_h, x \rangle_{\text{dec}} = \langle N_s | M_h, x \rangle_{\text{dec}}^2.$$

and thus that

$$\begin{aligned} \langle N_s(N_s - 1) | M_h \rangle_{\text{dec}} &= \int \langle N_s | M_h, x \rangle_{\text{dec}}^2 P(x | M_h) dx \\ &\neq \langle N_s | M_h \rangle_{\text{dec}}^2, \end{aligned} \quad (20)$$

Hence, in this case the *marginalized*, decorated HOD, $P_{\text{dec}}(N_g | M_h)$, cannot be Poissonian and Eq. (15) cannot be satisfied for $k = 2$ (i.e., one cannot conserve the second moment of the HOD).

As a second alternative, one could insist upon the principle of HOD conservation, $P_{\text{dec}}(N_s | M_h) = P_{\text{std}}(N_s | M_h)$, and assume $P_{\text{dec}}(N_s | M_h, x)$ to be Poissonian. In that case neither $P_{\text{dec}}(N_s | M_h)$ nor $P_{\text{std}}(N_s | M_h)$ can be Poissonian.

Third, still insisting on HOD conservation, one could choose for $P_{\text{std}}(N_s | M_h)$ to be Poissonian. Now one has that $P_{\text{dec}}(N_s | M_h)$ is Poissonian as well, but then of course $P_{\text{dec}}(N_s | M_h, x)$ cannot obey Poisson statistics for all x . As a simple, explicit demonstration of this last case, suppose that $P_{\text{dec}}(N_s | M_h, x)$ is such that

$$\langle N_s(N_s - 1) | M_h, x \rangle_{\text{dec}} = \alpha^2 \langle N_s | M_h, x \rangle_{\text{dec}}^2, \quad (21)$$

where α is a constant. Note that α cannot be equal to unity, which would correspond to $P_{\text{dec}}(N_s | M_h, x)$ being Poissonian. Eq. (17) now implies that

$$\alpha^2 = \left[1 + \int \frac{[\delta N_s^1(M_h, x)]^2}{\langle N_s | M_h, x \rangle_{\text{dec}}^2} P(x | M_h) dx \right]^{-1}. \quad (22)$$

Since the integral in the above expressions is non-negative, this implies that $\alpha^2 < 1$. Hence, *in order to conserve the HOD, the distribution $P_{\text{dec}}(N_s | M_h, x)$ must have a distribution that is narrower than a Poisson distribution with mean $\langle N_s | M_h, x \rangle_{\text{dec}}$.* The intuitive way of thinking of this result is that there is an additional source of variance associated with the allocation of satellites into

sub-populations at a given halo mass. Of course, introduction of the constant α is only one simple way in which to characterize $P_{\text{dec}}(N_s|M_h, x)$; in practice there is an infinite set of possible decorations that satisfy Eq. (17).

4.1.4 The central-satellite term

As discussed in §2.3, halo occupation models also need to make an assumption regarding $\langle N_c N_s \rangle$, which specifies the expectation value for the number of central-satellite pairs. Throughout this paper we assume that

$$\langle N_c N_s | M_h, x \rangle_{\text{dec}} = \langle N_c | M_h, x \rangle_{\text{dec}} \cdot \langle N_s | M_h, x \rangle_{\text{dec}}, \quad (23)$$

and thus that the occupation numbers for centrals and satellites *at fixed* M_h and x are independent. Note, though, that because of the mutual covariance with the secondary halo property x , this will generally *not* be the case for the corresponding marginalized moment, i.e.,

$$\begin{aligned} \langle N_c N_s | M_h \rangle_{\text{dec}} &= \int \langle N_c N_s | M_h, x \rangle_{\text{dec}} P(x|M_h) dx \\ &\neq \langle N_c | M_h \rangle_{\text{dec}} \cdot \langle N_s | M_h \rangle_{\text{dec}}. \end{aligned} \quad (24)$$

Assembly bias induces a non-trivial $\langle N_c N_s | M_h \rangle$ through the auxiliary property x . This assumption is not a necessary feature of the decorated HOD, and as described in §6 the **Halotools** framework is written to accommodate alternative assumptions for central-satellite correlations.

As discussed in more detail in §4.2 below, the decoration of centrals is limited by the requirement that $0 \leq \langle N_c \rangle \leq 1$. Consequently, if $\langle N_c | M_h \rangle_{\text{dec}} = 1$ (which is typically the case for massive halos), one also has that $\langle N_c | M_h, x \rangle_{\text{dec}} = 1$ (see §4.2 below), and thus

$$\langle N_c N_s | M_h \rangle_{\text{dec}} = \langle N_s | M_h \rangle_{\text{dec}}. \quad (25)$$

Similarly, if $\langle N_c | M_h \rangle_{\text{dec}} = 0$ (which is typically the case in low mass halos), then $\langle N_c | M_h, x \rangle_{\text{dec}} = 0$ and thus $\langle N_c N_s | M_h \rangle_{\text{dec}} = 0$. Hence, under HOD conservation, the average number of central-satellite pairs in massive halos for a decorated model is identical to that of its standard baseline model, except for the fairly narrow range in halo masses for which $0 < \langle N_c | M_h \rangle < 1$ (see also §5.1.1 and §5.3).

4.2 A Toy Model: Discrete Halo Sub-Populations

In this section we will develop a simple toy example of a decorated HOD in which the halo population at fixed mass is split into two sub-populations. For example, there is one sub-population that contains a fraction P_1 of all halos (the “type 1” halos) at fixed mass for which $\delta N_s(M_h, x) = \delta N_{s,1}$ (a constant) and a second population containing $P_2 = 1 - P_1$ of all halos at fixed mass and for which $\delta N_s(M_h, x) = \delta N_{s,2}$. This could be achieved by splitting the halo population into the P_1 percentile of highest- x halos and assigning them a satellite galaxy occupation enhancement of $\delta N_{s,1}$. Likewise, the remaining $1 - P_1$ percentile of lowest x halos receive a satellite galaxy occupation decrement of $\delta N_{s,2}$. This is a simple case of two, discrete halo sub-populations, with different occupation statistics, at fixed mass.

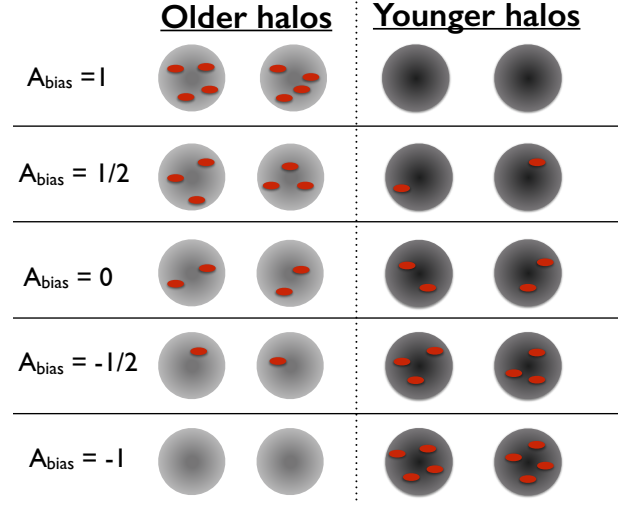


Figure 1. Cartoon illustration of the decorated HOD. Each row of circles represents a population of halos of the same mass, divided evenly on the left and right into halos that are old and young for their mass, respectively. The number of galaxies in each halo is represented with the small, red ellipses. As described in §4.2, the $\mathcal{A}_{\text{bias}}$ parameter governs the strength of assembly bias in our two-population model. Each row gives a visual representation of a different value of $-1 \leq \mathcal{A}_{\text{bias}} \leq 1$. More positive values of $\mathcal{A}_{\text{bias}}$ correspond to models in which later-forming halos host more galaxies relative to earlier-forming halos of the same mass, and conversely for $\mathcal{A}_{\text{bias}} < 0$. Note that changing values of $\mathcal{A}_{\text{bias}}$ does not change $\langle N_g | M_h \rangle$, the mean number of galaxies averaged across all halos of a fixed mass; this is the defining feature of the decorated HOD, and the meaning of the principle of HOD conservation.

In such a scenario, conserving the first moment of the HOD (Eq. [17], for $k = 1$) requires that

$$0 = P_1 \delta N_{s,1} + P_2 \delta N_{s,2}, \quad (26)$$

and likewise for centrals. As discussed in §4.1, the second central occupation moment is automatically conserved. For the satellites, we choose to assume that both $P_{\text{dec}}(N_s|M_h, x)$ and $P_{\text{std}}(N_s|M_h)$ are Poisson, and thus that the second occupation moment is not conserved. (see Mao et al. 2015, for the motivation for this choice based on subhalo occupation statistics). With these two assumptions, one need only specify the two first-order decoration functions, $\delta N_{c,1}$ and $\delta N_{s,1}$, and then $P_{\text{dec}}(N_g|M_h, x)$ is completely determined.

In order to guarantee that the mean number of galaxies is always non-negative and that the mean number of centrals is never greater than one, there is a restricted set of values which the decoration functions $\delta N_{s,1}$ and $\delta N_{c,1}$ may take on. It is easy to show that the maximum strength of assembly bias for satellites in this two-population toy model is

$$\delta N_{s,1}(M_h, x) \leq \delta N_{s,1}^{\text{max}}(M_h) = \frac{1 - P_1}{P_1} \langle N_s | M_h \rangle_{\text{std}}. \quad (27)$$

Eq. (27) ensures that $\langle N_s \rangle \geq 0$ in type-2 halos ($x < \bar{x}(M_h)$). The constraint that $\langle N_s \rangle \geq 0$ in type-1 halos

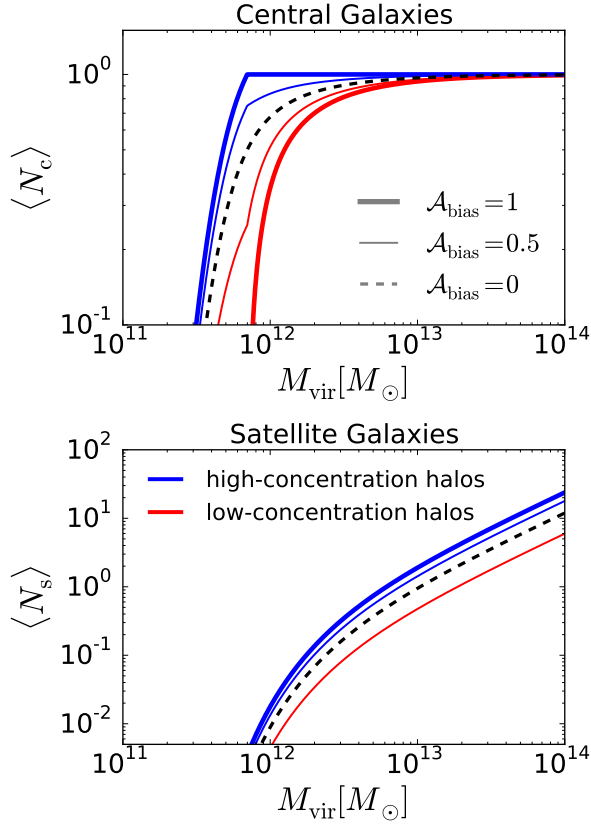


Figure 2. Decorated HOD occupation statistics. All curves pertain to the Leauthaud et al. (2011) HOD (see §2.4) with stellar mass threshold $M_* > 10^{10.5} M_\odot$ with $\sigma_{\log M_*} = 0.4$. The parameter $\mathcal{A}_{\text{bias}}$ controls the strength of assembly bias. The value $\mathcal{A}_{\text{bias}} = 1$ (thick blue and red curves) shows the case of maximum assembly bias allowed by the HOD-conservation constraint; $\mathcal{A}_{\text{bias}} = 0.5$ (thin blue and red curves) shows a model with 50% allowable strength; the standard HOD result $\mathcal{A}_{\text{bias}} = 0$ is shown with the dashed black curve. Assembly bias can have no impact on central occupation statistics in the $\langle N_{\text{cen}} \rangle = 1$ regime, whereas satellite occupations are unbounded and so can be biased at large halo mass. There is no thick red curve in the bottom panel because in the $\mathcal{A}_{\text{bias}} = 1$ model there are exactly zero satellites in high-concentration halos.

($x > \bar{x}(M_h)$) can be written as

$$\delta N_{s,1}(M_h, x) \geq \delta N_{s,1}^{\min}(M_h) = -\langle N_s | M_h \rangle_{\text{std}}. \quad (28)$$

Notice that the range of possible values for $\delta N_{s,1}$ depends upon both P_1 and the value of the first moment of the “baseline” model, $\langle N_s | M_h \rangle_{\text{std}}$. We return to this important point in the discussion of our results.

Central galaxies are subject to the same positivity constraint that $\langle N_c | M_h, x \rangle \geq 0$ as well as the additional constraint that the number of central galaxies in any halo can never exceed one, $\langle N_c | M_h, x \rangle \leq 1$. As a result, the maximum strength of assembly bias for centrals is given by

$$\delta N_{c,1}^{\max} = \min \left\{ 1 - \langle N_c | M_h \rangle_{\text{std}}, \frac{1 - P_1}{P_1} \langle N_c | M_h \rangle_{\text{std}} \right\}. \quad (29)$$

The minimum in Eq. (29) selects that constraint on the central population which is most restrictive. Ensuring that centrals in type-2 halos also respect $0 \leq \langle N_c | M_h, x \rangle \leq 1$ places the following constraint on centrals in type-1 halos

$$\delta N_{c,1}^{\min} = \max \left\{ -\langle N_c | M_h \rangle_{\text{std}}, \frac{1 - P_1}{P_1} (\langle N_c | M_h \rangle_{\text{std}} - 1) \right\}. \quad (30)$$

The quantities $\delta N_{c,2}$ and $\delta N_{s,2}$ are subject to the same constraints described by Eqs. (27)-(30). Note that when one population attains its maximum (minimum) allowed value, Eq. (26) guarantees that the other population automatically attains its minimum (maximum).

4.2.1 Defining the assembly bias parameter $\mathcal{A}_{\text{bias}}$

In the following sections, we give examples of the plausible strength of assembly bias effects based upon this simple, but illustrative, two-population model. In those sections, we refer to the strength of assembly bias using the parameter $-1 \leq \mathcal{A}_{\text{bias}}(M_h) \leq 1$. The $\mathcal{A}_{\text{bias}}$ parameter governs assembly bias in this two-population, decorated HOD as

$$\delta N_{g,1}(M_h) = \begin{cases} |\mathcal{A}_{\text{bias}}(M_h)| \delta N_{g,1}^{\max}(M_h) & : \mathcal{A}_{\text{bias}} > 0 \\ |\mathcal{A}_{\text{bias}}(M_h)| \delta N_{g,1}^{\min}(M_h) & : \mathcal{A}_{\text{bias}} < 0 \end{cases}$$

Thus in our nomenclature, the dimensionless $\mathcal{A}_{\text{bias}}$ parameter specifies the strength of assembly bias as a fraction of its maximum allowable effect. The maximum and minimum assembly bias strengths, $\delta N_{c,1}^{\max}$, $\delta N_{c,1}^{\min}$, $\delta N_{s,1}^{\max}$ and $\delta N_{s,1}^{\min}$, are given in Eqs. (27)-(30). Our sign convention is always to choose the “type-1” halos to be those in the upper-percentile of the secondary property (e.g., $x \geq \bar{x}(M_h)$). Fig. 1 is a cartoon illustration of a two-population scenario such as this one.

As a specific example, suppose we choose the secondary halo property x to be halo concentration, that we split our halo population in half at each halo mass, and that we wish for both centrals and satellites in halos with above-average concentration to receive a boost to their mean occupations by 50% of the maximum allowable strength at each mass. Then we have $P_1 = 0.5$, $\mathcal{A}_{\text{bias}} = 0.5$, and thus

$$\begin{aligned} \delta N_{s,1}(M_h) &= 0.5 \delta N_{s,1}^{\max} = 0.5 \langle N_s | M_h \rangle_{\text{std}} \\ \delta N_{s,2}(M_h) &= 0.5 \delta N_{s,2}^{\min} = -0.5 \langle N_s | M_h \rangle_{\text{std}}, \end{aligned}$$

with directly analogous equations holding for centrals.

Figure 2 shows examples of HODs constructed by splitting the host halo population in the Bolshoi simulation on halo concentration using $P_1 = 0.5$. Fig. 2 shows examples of galaxy assembly bias of strength $\mathcal{A}_{\text{bias}} = 0$ (no assembly bias, dashed black curves), $\mathcal{A}_{\text{bias}} = 1$ (maximum allowable assembly bias in a two-population model, thick red and blue curves), and an intermediate value of $\mathcal{A}_{\text{bias}} = 0.5$ (thin red and blue curves).

The top panel of Fig. 2 exhibits the HODs of central galaxies in this model. In the case of central galaxies, assembly bias is restricted to the regime $0 < \langle N_c \rangle < 1$. Thus the scatter in the stellar-to-halo-mass relation controls the operative halo mass range for central galaxy assembly bias; we will return to this point in §5.3.

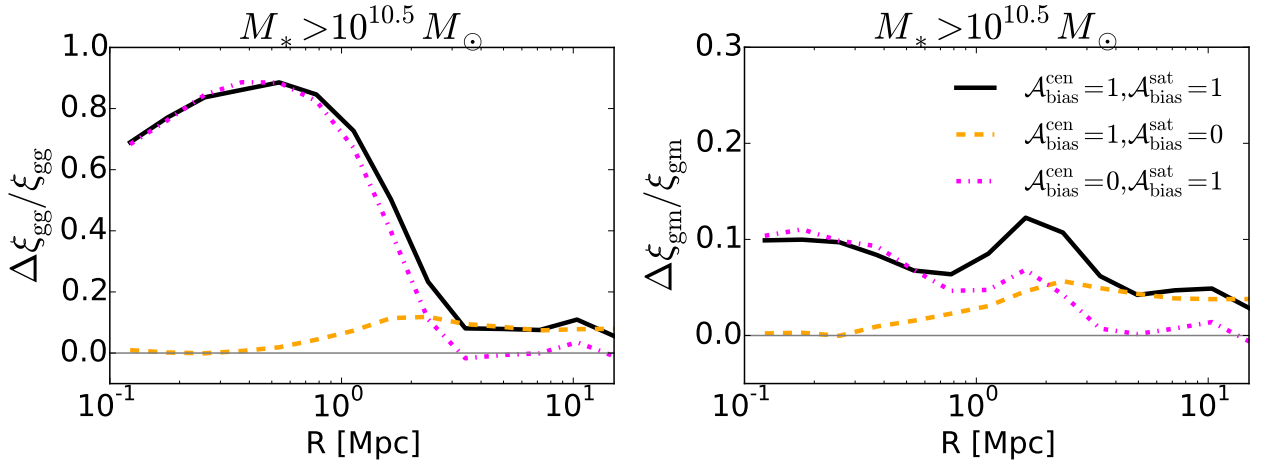


Figure 3. Parsing central and satellite assembly bias. The *left* panel shows the effect of assembly bias on galaxy clustering. The curves show the fractional change to ξ_{gg} as a function of spatial separation for three different assembly bias models. The *solid, black* line shows a model in which both centrals and satellites have maximum assembly bias of the same sign, $\mathcal{A}_{\text{bias}}^{\text{cen}} = \mathcal{A}_{\text{bias}}^{\text{sat}} = 1$. The *dashed, orange* lines shows the case of maximum assembly bias in the centrals, zero assembly bias in the satellites; conversely, the *dot-dashed, purple* line shows the effect of standard central occupations but maximum assembly bias in the satellites. The *right* panel is similar, but shows the fractional effect of these models on the galaxy-mass cross correlation.

The lower panel of Fig. 2 shows the effect of galaxy assembly bias on the satellites within the two host halo sub-populations. Unlike the case of central galaxies, satellite galaxy assembly bias is relevant at all host halo masses for which $\langle N_s | M_h \rangle_{\text{std}} > 0$. In particular, note that there is no thick red curve in the lower panel of Fig. 2. This is because in the $\mathcal{A}_{\text{bias}}^{\text{sat}} = 1$ case, there are exactly zero satellites in low-concentration halos. This is different for the $\mathcal{A}_{\text{bias}}^{\text{cen}} = 1$ case due to the constraint that a halo cannot be occupied by more than one central.

5 IMPACT OF ASSEMBLY BIAS ON CLUSTERING

In order to demonstrate the potential impact of assembly bias, we use *Halotools* to populate dark matter halos in the Bolshoi simulation with galaxies with a stellar mass $M_* > 10^{10.5} M_\odot$. We use the standard HOD model described in §2.4 as our ‘no-assembly-bias’ baseline model, which we decorate using a simply two-population model as follows. At each halo mass, we split the halo population into low- and high-concentration halos; those within the top 50% of concentration at fixed M_h are assigned to the first sub-population, and the remaining to the second population (so $P_1 = P_2 = 0.5$). With this choice, a *positive* value for $\mathcal{A}_{\text{bias}}$ implies that halos with above-average concentration have *boosted* galaxy occupations.⁶ We assume that both $P_{\text{std}}(N_s | M_h)$ and $P_{\text{dec}}(N_s | M_h, x)$ are Poisson distributions, so that the decorated HOD is entirely specified by two free parameters: $\mathcal{A}_{\text{bias}}^{\text{cen}}$ and $\mathcal{A}_{\text{bias}}^{\text{sat}}$.

⁶ This is opposite the intuitive expectation that high-concentration halos should have fewer satellites (Zentner et al. 2005). This more natural expectation simply corresponds to a negative value of $\mathcal{A}_{\text{bias}}$, and will be addressed in the next subsection.

When both of these parameters equal zero, the model is formally equivalent to the baseline ‘no-assembly-bias’ model of Leauthaud et al. (2011).

Once we have populated the Bolshoi simulation volume with mock galaxies, we compute the corresponding galaxy-galaxy and galaxy-matter correlation functions using the fast pair-counting facilities of *Halotools* combined with the Landy & Szalay (1993) correlation function estimator. Our figures can be reproduced in quantitative detail using the annotated IPython Notebook in the repository stored at <https://github.com/aphearin/decorated-hod-paper>. This repository also contains a frozen copy of the exact version of *Halotools* that generated our results.

5.1 Central vs. Satellite Assembly Bias

Figure 3 exhibits our first demonstration of the sense and size of assembly bias effects on two-point functions of galaxy samples in our simple two-population toy model. We explore three different models for the decoration that only differ in their treatment of centrals and satellites, and compare the resulting correlation functions to the corresponding signal in the baseline model:

- (i) $\mathcal{A}_{\text{bias}}^{\text{cen}} = 1, \mathcal{A}_{\text{bias}}^{\text{sat}} = 1$, maximum assembly bias in both populations (*black curves*).
- (ii) $\mathcal{A}_{\text{bias}}^{\text{cen}} = 1, \mathcal{A}_{\text{bias}}^{\text{sat}} = 0$, maximum central assembly bias only (*dashed, yellow curves*).
- (iii) $\mathcal{A}_{\text{bias}}^{\text{cen}} = 0, \mathcal{A}_{\text{bias}}^{\text{sat}} = 1$, maximum satellite assembly bias only (*dot-dashed, magenta curves*).

Note how assembly bias in satellites vs. centrals imprints a distinct signature on galaxy clustering as well as lensing, as we discuss in more detail what follows.

5.1.1 Small-scale ($R \lesssim 1\text{Mpc}$) clustering

Interestingly, the small- and large-scale influences of assembly bias on galaxy clustering can be qualitatively different. From the close agreement between the solid, black and dot-dashed, magenta curves in Fig. 3, it is evident that for large values of $\mathcal{A}_{\text{bias}}$, the influence of satellite assembly bias dominates that of centrals on small scales.

We can understand this through the analytical halo-model expression, Eq. (1). The one-halo term has two contributions: one from $\langle N_c N_s \rangle$, and another from $\langle N_s (N_s - 1) \rangle$. The central-satellite term may only be altered by a small amount due to assembly bias. This is because we have assumed that the occupation statistics of centrals and satellites obey Eq. (23). Consequently, as discussed in §4.1.4, the halo mass range over which assembly bias can influence central galaxy occupation at all is limited to host halo masses where $0 < \langle N_c | M_h \rangle_{\text{std}} < 1$. This range is typically fairly narrow, as is evident in the top panel of Fig. 2, and because halos of these masses typically have zero satellite galaxies, the expectation value $\langle N_c N_s \rangle$ is left nearly unaffected by assembly bias.

This is the behavior that is typical of most M_* -threshold HODs explored in the literature as reasonable descriptions of observational data; however, exceptions to this reasoning may be realized, particularly for samples selected such that $\langle N_c | M_h \rangle_{\text{std}} < 1$ while $\langle N_s | M_h \rangle_{\text{std}} > 0$ over a broad range of halo masses. For a commonly encountered example, see the blue-selected galaxy HODs inferred by Zehavi et al. (2011) or discussed in the mock catalogs of Zentner et al. (2014).

The boost in small-scale clustering due to assembly bias is nearly entirely due to an increase in the number of satellite-satellite pairs (an increase in the $\langle N_s^2 \rangle$ term in the halo model) for relatively high-mass host halos. This effect is simple to understand. Packing the same number of satellites into fewer hosts increases the average number of pairs per host and decreases the number of relevant hosts. This leads to a significant boost in small-scale clustering (see Watson et al. 2011) as the same number of galaxies are apportioned among fewer, richer groups. This dependence should be fairly generic.

Finally we point out that since we have assumed that satellite galaxies trace the dark matter, i.e., $n_{\text{sat}}(r)$ is modeled as a NFW profile with the same concentration parameter as for the dark matter host halo, implementing assembly bias via a split on host halo concentration modifies the average, satellite-number-weighted, number density profile of satellite galaxies. However, this has only a very small impact on the clustering signal, which is completely dominated by changes in the typical number of satellite-satellite pairs. In other words, the shift in clustering on small scales is dominated by the changes in $\langle N_s^2 \rangle$, and would be present even if we had divided our host halo sample into two random sub-populations at fixed mass (see Paranjape et al. 2015, section 2, for a discussion of this same point in a different context).

5.1.2 Large-scale ($R > 1\text{Mpc}$) clustering

On large scales, the distinct signatures of central vs. satellite assembly bias arise from different considerations. For

host halos whose mass is below the non-linear collapse mass, $M_{\text{coll}} \approx 10^{12.7} M_\odot$, high-concentration halos exhibit a larger clustering bias relative to low-concentration halos of the same mass. This trend weakens with increasing halo mass and may even change sign for halos with $M_h \gg M_{\text{coll}}$ (Wechsler et al. 2006), such that for halos with masses greater than the collapse mass it is the low-concentration halos that cluster more strongly. Large-scale galaxy clustering is a weighted average of halo clustering (see Eq. [2]) and the role of *galaxy assembly bias* on large scales is in determining the weighting of halo-halo pairs. Apportioning more galaxies into a subset of halos that is more strongly clustered will weight those halos more highly and boost clustering, whereas preferentially placing galaxies into a subset of halos that clusters more weakly at fixed mass will suppress clustering.

Figure 3 demonstrates that central galaxy assembly bias has a far more important influence on the two-halo term relative to satellite galaxy assembly bias. This is due to two distinct effects. First and foremost, centrals dominate satellites by number; for the stellar mass threshold of $M_* > 10^{10.5} M_\odot$ shown here, more than 75% of galaxies are centrals. So central-central pairs are far more common than central-satellite or satellite-satellite pairs in the two-halo regime (see Watson et al. 2011) and altering central galaxy occupations induces greater deviations in large-scale clustering.

Second, satellites preferentially occupy more massive halos than the vast majority of central galaxies in most samples (see Fig. 2). For our particular example, which represents galaxies with stellar mass $M_* > 10^{10.5} M_\odot$, $\sim 75\%$ of satellites occupy host halos with masses $M_h > 10^{13} M_\odot$. The majority of satellites in this sample occupy hosts with masses greater than the collapse mass, $M_{\text{coll}} \approx 10^{12.7} M_\odot$, for which halo assembly bias is markedly weaker (and perhaps of opposite sense) than the assembly bias of lower-mass host halos. Consequently, altering the weighting of halos that are large enough to host satellite galaxies produces only very modest changes in large-scale clustering. As with our discussion of the influence of assembly bias on small-scale clustering, these considerations should be fairly typical for the vast majority of HODs explored in the literature. However, assembly bias will lead to different effects if the galaxy sample is selected in such a way that the satellite fraction is particularly large and/or halos with masses $M_h \ll M_{\text{coll}}$ host satellites in significant numbers.

5.1.3 Galaxy-galaxy lensing

Now consider the right-hand panel of Figure 3. This panel shows the influence of galaxy assembly bias on the galaxy-matter cross correlation, the fundamental two-point statistic underlying the galaxy-galaxy lensing signal. On large scales ($R \gg 1\text{Mpc}$), the physical picture discussed in § 5.1.2 is unchanged: the signal can be understood entirely in terms of the relative weighting of halo-halo pairs, and central galaxy assembly bias dominates the effect in this regime.

On small scales $R \sim 100 - 400$ kpc, the $\langle N_s^2 \rangle$ boost discussed in § 5.1.1 is not relevant because the

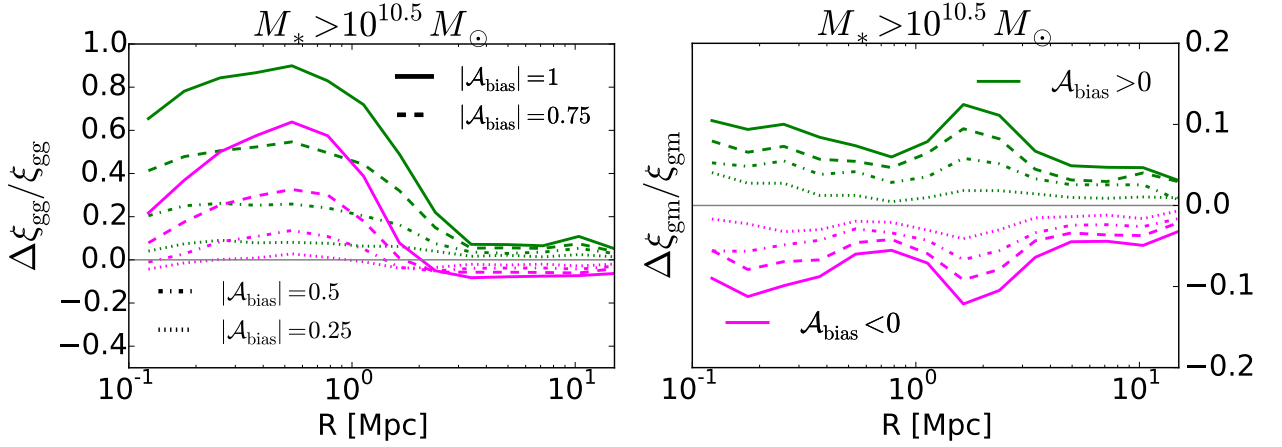


Figure 4. Varying the strength of assembly bias. Impact of assembly bias on galaxy-galaxy clustering (left) and the galaxy-mass cross correlation (right). The strength of the assembly bias is shown in the legend in the *left* panel. Green curves show results for $\mathcal{A}_{\text{bias}} > 0$, in which case high-concentration halo occupations are boosted relative to low-concentration halos of the same mass; magenta curves show the opposite case of $\mathcal{A}_{\text{bias}} < 0$. All curves pertain to a baseline, mass-only HOD with stellar mass threshold $M_* > 10^{10.5} M_\odot$ with $\sigma_{\log M_*} = 0.4$, as in Figures 2 & 3. Notice that the effects of assembly bias, even in this simple toy model, are potentially large and complex. Furthermore, note that under the assumptions of this model, in the pure one-halo regime assembly bias always boosts galaxy-galaxy clustering (but *not* necessarily the galaxy-mass cross correlation).

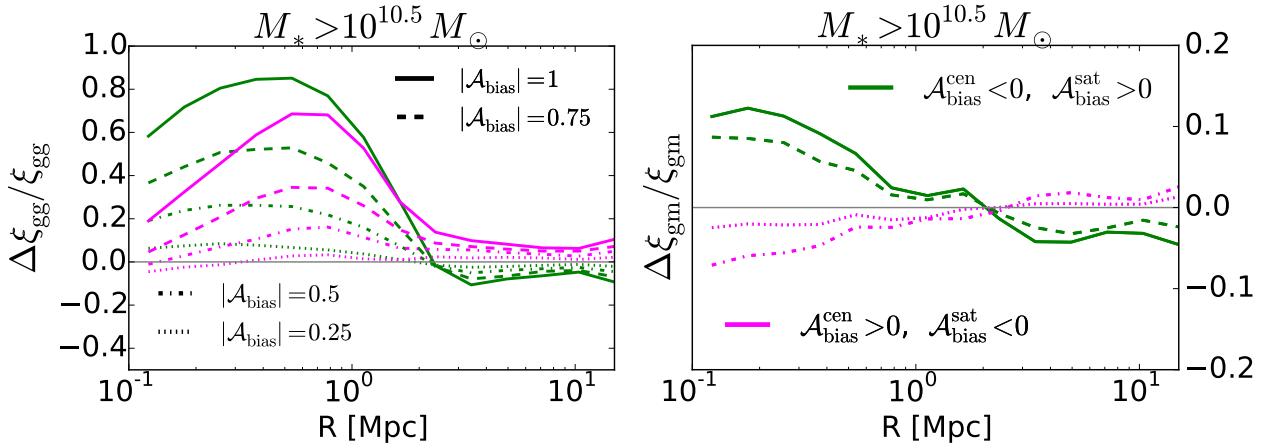


Figure 5. Same as Fig. 4, but central and satellite assembly bias have opposite sign.

galaxy-matter cross correlation is sensitive to galaxy-matter “pairs,” not galaxy-galaxy pairs. Instead, in this regime, there are two contributions to the clustering: one proportional to $\langle N_c | M_{\text{vir}} \rangle$ and another proportional to $\langle N_s | M_{\text{vir}} \rangle$. For both contributions, the one-halo term of galaxy-matter clustering is a probe of the halo mass profile, and so we should naturally expect that preferentially populating halos with high-concentration profiles should boost ξ_{gm} in the one-halo regime.

The right-hand panel of Figure 3 shows that this expectation is born out: the galaxy-matter cross correlation gets a $\sim 10\%$ boost on $R \lesssim 400 \text{ kpc}$ when $\mathcal{A}_{\text{bias}} = 1$. Perhaps not surprisingly, we can see that this effect is far more important for satellite galaxies than for centrals. Referring to Eq. (3), we can see that there are two distinct effects responsible for this difference. The first effect is due to the different spatial distributions of centrals and

satellites. Because we model satellite galaxies to trace the underlying dark matter potential, then by boosting satellite occupations in high-concentration halos, both $\rho_m(r)$ and $n_{\text{sat}}(r)$ get a boost to the effective concentration parameter, c_{eff} . The convolution factor Ξ_{gm} in the $\langle N_s | M_{\text{vir}} \rangle$ term therefore gets a boost that is quadratic in c_{eff} . Central galaxies, on the other hand, are assumed to sit at the halo center, and so the Ξ_{gm} factor in the $\langle N_c | M_{\text{vir}} \rangle$ term is only boosted in linear proportion to c_{eff} .

The second reason central and satellite assembly bias have distinct contributions to one-halo lensing has to do with the combinatorics of assembly bias. As discussed in § 5.1.1, the halo mass range over which assembly bias can influence central galaxy occupations is restricted by the constraint that $0 < \langle N_c \rangle < 1$; as a result, central assembly bias for our fiducial $M_* > 10^{10.5} M_\odot$ sample ceases to be operative for $M_{\text{vir}} \gtrsim 5 \times 10^{12} M_\odot$ (see Fig. 2).

Hence, it is not possible for central occupation assembly bias in this sample to have any effect at all on scales $R \gtrsim R_{\text{vir}}(M_{\text{vir}} = 5 \times 10^{12} M_{\odot}) \approx 350 \text{ kpc}$.

Finally, the one-to-two-halo transition region on scales $R \sim 1 - 3 \text{ Mpc}$ exhibits a marked “bump” feature, with contributions from both centrals and satellites. As first pointed out in Sunayama et al. (2015), this characteristic scale-dependent signature of assembly bias is associated with so-called “splashback” material that is physically bound to the halos of massive groups and clusters and is congregating at the point of first apocentric passage (Adhikari et al. 2014; Diemer & Kravtsov 2014; More et al. 2015). In fact, this signature can also be seen in the dashed, yellow curve in the left-hand panel of Figure 3, but it is not visible in either the black or dot-dashed magenta curves because it is swamped by the $\langle N_s^2 \rangle$ boost discussed in §5.1.1.

5.2 The Strength of Assembly Bias

A practical conclusion from the results presented in Fig. 3 is that galaxy assembly bias can potentially be a very significant effect compared to the standards of contemporary and future measurements of galaxy clustering and lensing. Even in this simple model, the shift in large-scale clustering of galaxies can be as large as $\sim 10\%$. Moreover, the effect is strongly scale dependent and assembly bias can cause a change in small-scale clustering strength of nearly a factor of ~ 2 . Likewise, the galaxy-mass cross correlation can plausibly be shifted by $\sim 10\%$ or more by assembly bias and that shift may have non-trivial scale dependence.

In § 5.1.3 we restricted attention to the case where assembly bias in centrals and satellites is of maximum strength and of the same positive sign. In this section we study how variations in both the strength and sign of $\mathcal{A}_{\text{bias}}$ manifest in galaxy clustering and lensing. Various assembly bias strengths $\mathcal{A}_{\text{bias}}$ are depicted in Fig. 4. In these examples, both the central galaxy and satellite galaxies are assigned the same values of $\mathcal{A}_{\text{bias}}$ and in all cases the baseline HOD is, once more, the model described in § 2.4.

Perhaps even more intriguing than the dynamic range of assembly bias effects on large and small scales is the fact that the small-scale galaxy-galaxy clustering shift is *always positive* while the large-scale shift in the galaxy correlation function induced by assembly bias can be of either sign. The large-scale galaxy clustering can be thought of as a weighted average of the halo bias (cf., the term in brackets in Eq. [2]). Shifting galaxies away from weakly-clustered host halos toward strongly-clustered host halos increases the overall galaxy clustering signal and vice versa. Therefore, assembly bias can induce either an increment or a decrement on large-scale clustering. Contrarily, on small scales, as discussed in § 5.1.1, the signal is dominated by satellite-satellite pairs and shifting a fixed total number of satellite galaxies into fewer host halos *always* increases $\langle N_s^2 \rangle$.

Figure 5 is analogous to Figure 4, except that in Fig. 5 the central and satellite assembly biases are of opposite sign (e.g., $\mathcal{A}_{\text{bias}}^{\text{cen}} = -\mathcal{A}_{\text{bias}}^{\text{sat}}$). Comparing the left

and right panels in Fig. 4 and Fig. 5, it is evident that the physical principles discussed in § 5.1 result in qualitatively different relative effects on large- and small-scales between ξ_{gg} and ξ_{gm} . Assembly bias can induce numerous changes to two-point statistics and these shifts can be of a wide range of amplitudes and scale dependences. However, as a consequence of this, simultaneous measurements of both galaxy-galaxy and galaxy-matter clustering over a wide range of length scales may, in principle, enable one to determine both the sign and amplitude of assembly bias. Further degeneracy breaking may be possible through the distinct manifestations of the “bump” feature at $R \sim 1 - 2 \text{ Mpc}$ in galaxy clustering and galaxy-galaxy lensing. We defer further discussion of these points to § 6.

5.3 Dependence Upon Baseline HOD

The degree to which assembly bias alters galaxy clustering statistics can be quite sensitive to the underlying baseline, mass-only, HOD of the galaxy population under consideration. In particular, the impact of assembly bias on ξ_{gg} is quite sensitive to the steepness of the transition from $\langle N_c | M_h \rangle_{\text{std}} = 0$ at low host masses to $\langle N_c | M_h \rangle_{\text{std}} = 1$ at high host masses. This steepness is controlled by the level of stochasticity in the central galaxy stellar mass at fixed halo mass, parameterized in our baseline model by $\sigma_{\log M}$ in Eq. (8).

This sensitivity to the underlying mass-only HOD can be understood quite simply. First, in typical samples, central galaxies constitute $\sim 70\% - 90\%$ of the sample, so the behavior of centrals is of primary importance⁷. If $\langle N_c | M_h \rangle_{\text{std}} = 0$, then there are no galaxies at all to be apportioned to specific halos according to a secondary property other than halo mass. If $\langle N_c | M_h \rangle_{\text{std}} = 1$, then all halos of that mass contain a central galaxy and again, there is only one way in which these galaxies can be apportioned among the halos of fixed mass. The flexibility to apportion central galaxies to halos according to a secondary property other than mass is available only when $\langle N_c | M_h \rangle_{\text{std}} > 0$ and $\langle N_c | M_h \rangle_{\text{std}} < 1$. The greater the range of host halo masses over which this condition is met, the larger the fraction of the sample that is subject to assembly bias. Therefore, increasing $\sigma_{\log M}$ increases the potential importance of assembly bias, particularly on large scales.

The importance of the baseline mass-only HOD, in particular the parameter $\sigma_{\log M}$, is shown in Figure 6. In Fig. 6, and in all subsequent figures, we choose to represent assembly bias with $\mathcal{A}_{\text{bias}}^{\text{cen}} = 1$ and $\mathcal{A}_{\text{bias}}^{\text{sat}} = 0.2$ so as to depress the strong small-scale influence of satellite assembly bias relative to the more mild large-scale influence of central galaxy assembly bias. These parameters designate our “fiducial” model of assembly bias for this and forthcoming comparisons.

Notice in Fig. 6 that the large-scale clustering of the sample can be enhanced by more than 15 – 20% for large

⁷ This is not necessarily true and could be violated if the galaxy selection function is tailored to favor satellites.

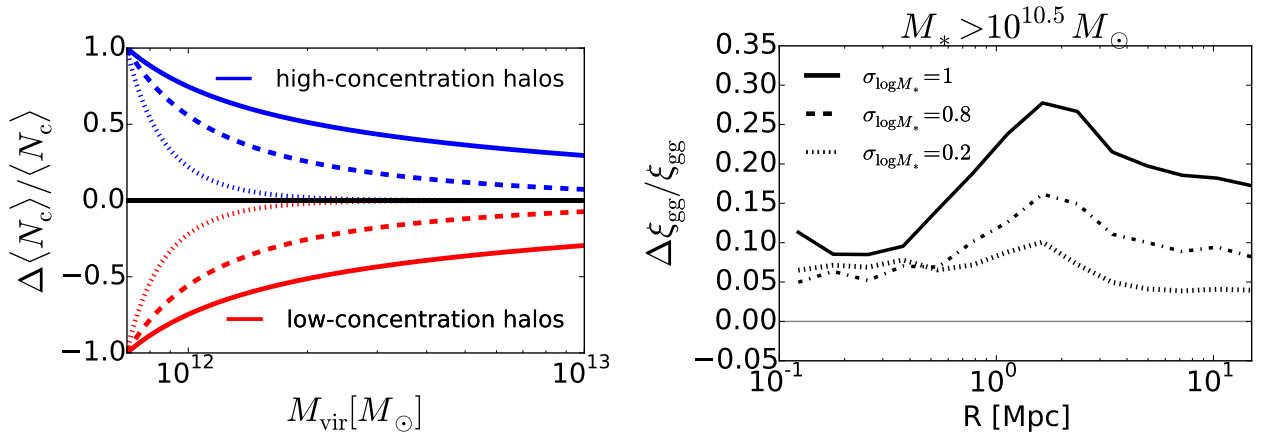


Figure 6. The role of scatter in the stellar-to-halo mass relation. The *left* panel shows the fractional difference in the central galaxy halo occupation in our simple model of galaxy assembly bias for various values of $\sigma_{\log M}$. Larger values of the scatter increase the dynamic range over which $0 < \langle N_c | M_h \rangle < 1$, creating a longer baseline in halo mass for assembly bias to be operative. In these figures, the assembly bias strength is set as $\mathcal{A}_{\text{bias}}^{\text{cen}} = 1$ and $\mathcal{A}_{\text{bias}}^{\text{sat}} = 0.2$. The *right* panel exhibits the deviations in galaxy clustering at various values of $\sigma_{\log M}$.

values of $\sigma_{\log M}$, whereas assembly bias effects are relatively small ($\sim 5\%$ or less) for $\sigma_{\log M} \lesssim 0.2$. This fact is especially interesting in light of the findings presented in Zentner et al. (2014): in HOD analyses of galaxy samples in which significant levels of assembly bias are erroneously ignored, one may infer erroneously small values of the $\sigma_{\log M}$ parameter ($\sigma_{\log M} \lesssim 0.2$) when the true underlying values are actually large (e.g., $\sigma_{\log M} \gtrsim 0.8$). Therefore, performing a standard HOD analysis on a sample and concluding that $\sigma_{\log M} < 0.2$ is not sufficient to render assembly bias effects to be on the order of a few percent or less (see Zentner et al. 2014, for detailed discussion of this point).

5.4 Dependence Upon Secondary Halo Property

In the previous subsections, we illustrated assembly bias using halo concentration, c , at fixed halo mass as the secondary halo property used to condition the HOD; however, halo clustering is now known to depend upon a number of halo properties and it is not clear which, if any, secondary halo property should be most closely related to galaxy properties. Numerous quantities may be sensible to explore in this context and in this section we demonstrate the induced galaxy assembly bias upon conditioning the HOD on a small subset of these host halo properties.

Measures of halo formation time are sensible halo properties on which to condition the HOD, particularly because it is not unreasonable to suspect that the formation history of a halo may be related in some way to the formation histories of the galaxies that the halo contains. We examine two properties associated with the formation histories of halos. First, we explore assembly bias induced by conditioning the HOD on the half-mass formation time of the host halo, $a_{1/2}$. As this name suggests, $a_{1/2}$ is the scale-factor at which the mass of the

host halo’s main progenitor first exceeded half the mass of the host halo at $z = 0$. Second, we condition HODs by the accretion rate of the halos, dM_h/dt , defined as the change in virial mass of the main progenitor halo over the past dynamical time $\tau_{\text{dyn}} \approx 2$ Gyr.

The assembly bias induced by these measures of halo formation history are shown as the green, dotted (for $a_{1/2}$) and magenta dot-dashed (for dM_h/dt) curves in Fig. 7. In both cases, assembly bias reduces the large-scale clustering strength of galaxies. We remind the reader of our sign convention: when $\mathcal{A}_{\text{bias}} > 0$, assembly bias boosts the occupation of halos with above average values of the secondary halo property at fixed mass. Formation time is anti-correlated with concentration (higher concentrations lead to earlier formation times and thus smaller values of either $a_{1/2}$ or dM_h/dt), so this result is qualitatively in accord with naive expectations.

Notice that on small scales ($r \lesssim 1$ Mpc), assembly bias induced by $a_{1/2}$ and dM_h/dt leads to an enhancement in galaxy clustering rather than a decrement. This is primarily driven by the $\langle N_s^2 \rangle$ boost effect described in § 5.1: assembly bias of this kind always packs satellite galaxies into fewer host halos, enhancing small-scale clustering.

However, small-scale clustering is also sensitive to a secondary effect related to the spatial profiles. When the sign of $\mathcal{A}_{\text{bias}}$ is positive, more galaxies are packed into halos with above-average values for the secondary property. For our fiducial case where the secondary property is halo concentration, $x = c$, this results in an *additional* boost to the two-point function because the effective spatial distribution of satellites and dark matter is boosted (this manifests itself in the $\Xi(r)$ term in Eqs. [1] and [3]). Because $a_{1/2}$ and dM_h/dt are anti-correlated with c , this spatial profile effect partially counteracts the $\langle N_s^2 \rangle$ boost described above, and so the weaker one-halo enhancement seen in these models relative to our fiducial c -based model is expected on these grounds. Of course,

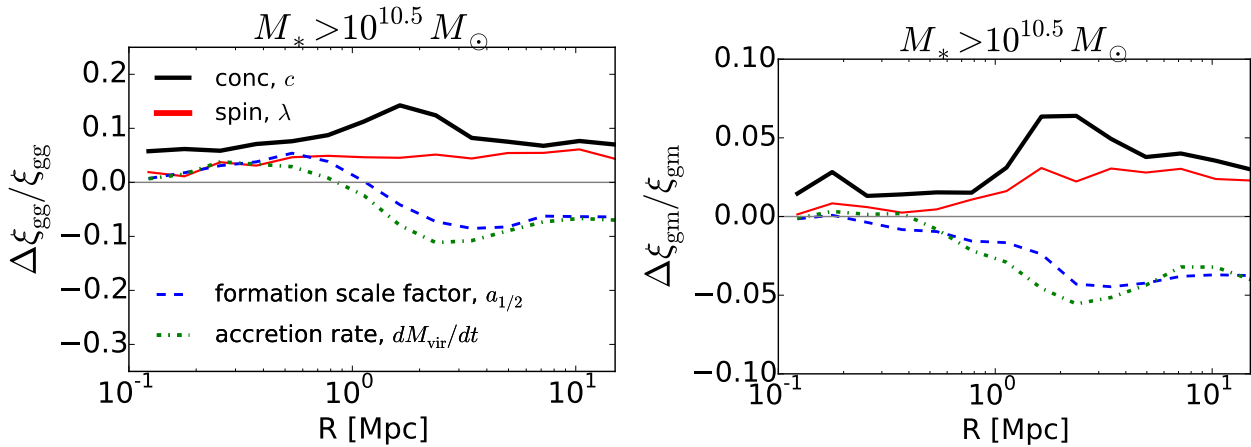


Figure 7. The role of the secondary halo property driving assembly bias. As in Fig. 6, we set the assembly bias strength parameters as $\mathcal{A}_{\text{bias}}^{\text{cen}} = 1$ and $\mathcal{A}_{\text{bias}}^{\text{sat}} = 0.2$; here our baseline HOD is for a $M_* > 10^{10.5} M_\odot$ threshold sample with $\sigma_{\log M} = 0.4$. Our sign convention is such that when $\mathcal{A}_{\text{bias}} > 0$, assembly bias boosts the occupation of halos with above average values of the secondary halo property. We choose different secondary halo properties to modulate galaxy occupation statistics as indicated in the legend.

the relations between halo formation time measures and concentration themselves exhibit significant scatter, so other factors may also contribute to this distinction.

As a final example, we demonstrate assembly bias induced by conditioning the HOD on the angular momentum of the host halo. To be specific, we condition the HOD on the halo spin parameter,

$$\lambda = \frac{J \sqrt{|E|}}{G M_h^{5/2}}, \quad (31)$$

where J is the total angular momentum of the halo and E is the total energy of the halo in a system defined such that the potential energy at infinity is zero (and therefore E is negative because halos are bound objects). The spin parameter is the ratio of the rotational kinetic energy of the system to the total kinetic energy of the halo and serves as a measure of the importance of rotation, as opposed to random motion, in supporting the system against gravitational collapse. The red, thin, solid lines in Fig. 7 show the galaxy assembly bias imposed by conditioning the HOD on λ in our simple two-population model.

As can easily be seen, although halo spin is correlated with halo formation and halo concentration, the large-scale galaxy assembly bias is considerably milder upon conditioning on λ than it is upon conditioning on c , $a_{1/2}$, or dM_h/dt . Consequently, the scale-dependence of the assembly bias induced by selecting on halo spin differs from the previous cases and is markedly weaker.

5.5 Mass and Redshift Dependence of Assembly Bias

In the previous sections, we explored assembly bias for a specific HOD model designed to approximate a sample of galaxies selected on a stellar mass threshold of $M_* > 10^{10.5} M_\odot$ at $z \approx 0$. The strength of the assembly bias of halos varies with both halo mass and redshift

and so it is instructive to examine examples of various mass thresholds at various epochs.

5.5.1 Stellar Mass Dependence

In the left panel of Figure 8 we use our fiducial model to study how the impact of assembly bias on galaxy clustering depends on the stellar mass threshold of the sample. Assembly bias of dark matter halos generically weakens with increasing halo mass (Wechsler et al. 2006), and in our HOD model M_* increases monotonically with M_h . Thus at fixed assembly bias parameter strength $\mathcal{A}_{\text{bias}}$, we should expect the impact of assembly bias on ξ_{gg} on large scales to become weaker in galaxy samples with higher stellar mass thresholds.

While the red curve in the left panel of Figure 8 shows that this is true for the $M_* > 10^{11.25} M_\odot$ sample, the clustering of the $M_* > 10^{10.75} M_\odot$ sample appears to be slightly *more* sensitive to assembly bias relative to the $M_* > 10^{10.25} M_\odot$ sample. We attribute this surprising result to insufficient resolution of the Bolshoi simulation. As shown in Figure 2 of Sunayama et al. (2015), Bolshoi exhibits non-monotonic behavior in the variation of halo assembly bias strength with halo mass for $M_{\text{vir}} \lesssim 10^{11.7} M_\odot$. Naively, this may be surprising since this corresponds to a halo with more than 3000 particles, vastly exceeding the industry convention of deeming halos with several hundred particles to be adequately resolved. However, we remind the reader that for models in which assembly bias is governed by concentration (or in the case of Sunayama et al. (2015), V_{max}), one must resolve the halo's internal structure, not just the halo itself. For halos with $M_{\text{vir}} \approx 10^{11.7} M_\odot$, the mean concentration is roughly ten. For such a concentration, the mass inside the scale radius is over ten times less than the total halo mass. Resolving the scale radius of such halos should therefore result in a tenfold increase in the simulation resolution requirements. For the $M_* > 10^{10.25} M_\odot$ sample,

$\sim 10\%$ of the centrals in the sample reside in halos with $M_{\text{vir}} < 10^{11.7} M_{\odot}$, whereas for the $M_* > 10^{10.75} M_{\odot}$ sample this fraction is less than 0.1%. We consider these estimates to be highly suggestive that Bolshoi suffers from resolution effects for this particular science target, though we leave a proper numerical resolution study as a subject for future investigation.

The M_* –dependence of small-scale clustering displays complex behavior that can again be understood using the physical considerations of §5.1. The small-scale assembly bias of the $M_* > 10^{11.25} M_{\odot}$ sample begins to overtake the effect seen in the other two samples on scales $R \lesssim 400 \text{ kpc}$, which corresponds to the virial radius of a halo of mass $M_{\text{vir}} \approx 5 \times 10^{12} M_{\odot}$. For the two lower mass thresholds, $\langle N_c \rangle = 1$ at this mass, whereas for the $M_* > 10^{11.25} M_{\odot}$ sample, $\langle N_c \rangle \approx 0.25$. Thus in the highest threshold sample, $\xi_{\text{gg}}(R \approx 400 \text{ kpc})$ actually receives a significant contribution from central-central and central-satellite pairs in halos where assembly bias is significant, whereas the statistics of HOD conservation prohibits the lower M_* –threshold samples from receiving such a contribution. This boosts the small-scale clustering effect of the $M_* > 10^{11.25} M_{\odot}$ sample relative to the other two.

5.5.2 Redshift Dependence

The right panel of Figure 8 shows that at fixed strength $\mathcal{A}_{\text{bias}}$, the impact of assembly bias on galaxy clustering weakens for galaxy samples at higher redshift. This effect is straightforward to understand. Over the range $z \lesssim 1$, there is very little evolution in the stellar-to-halo-mass relation (e.g., Behroozi et al. 2013). For example, in the Leauthaud et al. (2011) HOD model, the mean halo mass for a central galaxy of $M_* \approx 10^{10.5} M_{\odot}$ is $M_{\text{vir}} \approx 10^{11.9} M_{\odot}$ at $z = 0$ and $M_{\text{vir}} \approx 10^{12.1} M_{\odot}$ at $z = 1$. However, it is not the *absolute* mass M_{vir} that sets the strength of halo assembly bias, but rather the mass relative to the collapse mass M_{coll} . At $z = 0$, the collapse mass $M_{\text{coll}} \approx 10^{12.7} M_{\odot}$, but by redshift $z = 1$, the collapse mass has declined to $\sim 3 \times 10^{11} M_{\odot}$. So by comparing ξ_{gg} for samples at different redshift at fixed M_* , we are effectively comparing ξ_{gg} of halos with quite different values of $M_{\text{vir}}/M_{\text{coll}}$ (see Hearin et al. 2015, for an alternative discussion of this point in the context of galactic conformity). This effect is purely monotonic, and indeed we can see the impact of assembly bias is considerably weaker at $z = 1$ in $M_* > 10^{10.5} M_{\odot}$ samples relative to the present day.

6 DISCUSSION

In this paper, we have described a new analytical formalism, the decorated HOD, for encoding the effects of assembly bias on the galaxy-halo connection. For the sake of definiteness, we have chosen to focus on a simple toy model implementation of the decorated HOD in which halos of a given mass are divided into two sub-populations based on some secondary halo property. We have used this simple implementation to enumerate the primary set of effects that assembly bias can have on two-point clustering of stellar-mass threshold galaxy samples. In §6.1,

we describe how the scope of the decorated HOD framework is far broader than the toy model implementation in this work, and in §6.2 we compare the decorated HOD to previous attempts to encode assembly bias effects into galaxy-halo modeling. We conclude in §6.3 with a discussion of the relevance of this work to the precision-cosmology program.

6.1 Generality of the Decorated HOD Framework

In §4.1, we wrote the mean number of galaxies in a halo of mass M_h and some secondary property x as

$$\langle N_g | M_h; x \rangle \equiv \langle N_g | M_h \rangle + \delta N_g(M_h; x).$$

For any given “mass-only” HOD model describing $\langle N_g | M_h \rangle$, we can construct new “decorated” versions of such a model. We further suggested that in order to isolate the effects of assembly bias, it may be useful to assume that the decorated HOD satisfies “HOD conservation,” which we defined as $P_{\text{dec}}(N_g | M_h) = P_{\text{std}}(N_g | M_h)$, i.e., the marginalized probability function of the decorated HOD reduces to that of the baseline model. In practice, the HOD is used most often to model two-point statistics for which only the first two moments of the HODs are needed. As we describe below, the concepts of HOD decoration and conservation have many potential applications.

6.1.1 Decoration of arbitrary galaxy properties

The decorated HOD framework is not limited to applications concerning the prediction of $\langle N_g \rangle$. As stated above, the notion of “HOD conservation” implies a mathematical condition on the decoration function $\delta N_g(M_h; x)$ such that the value of $\langle N_g | M_h \rangle$ of the baseline model is left unchanged by the decoration.⁸ *This concept applies to any one-point function in the galaxy-halo connection, $\langle f | M_h \rangle$, not just $\langle N_g | M_h \rangle$.*

For example, if $\langle f | M_h \rangle = F_{\text{red}}^{\text{sat}}(M_h)$ is the red fraction of satellites as a function of halo mass, then the decorated HOD can be used to introduce assembly bias in the colors of satellites. In this case, we “decorate the red fraction,” instead of $\langle N_g \rangle$, and our first-moment conservation equation becomes

$$0 = \int \delta F_{\text{red}}^{\text{sat}}(M_h, x) P(x | M_h) dx.$$

By modeling the clustering and lensing of red galaxies as function of luminosity or stellar mass, such an approach can provide valuable insight as to which halo properties are most strongly correlated with satellite quenching.

We list a few further examples below to demonstrate the power of this generalization:

- (i) Let $x = t_{\text{imm}}$ be the time since the halo’s last major merger and let $\langle f | M_h \rangle$ express the average morphology of central galaxies (for example, let f correspond to the Sersic index n that best fits the galaxy’s

⁸ For brevity we focus exclusively on the first-order moments here, but everything extends trivially to higher orders as well.

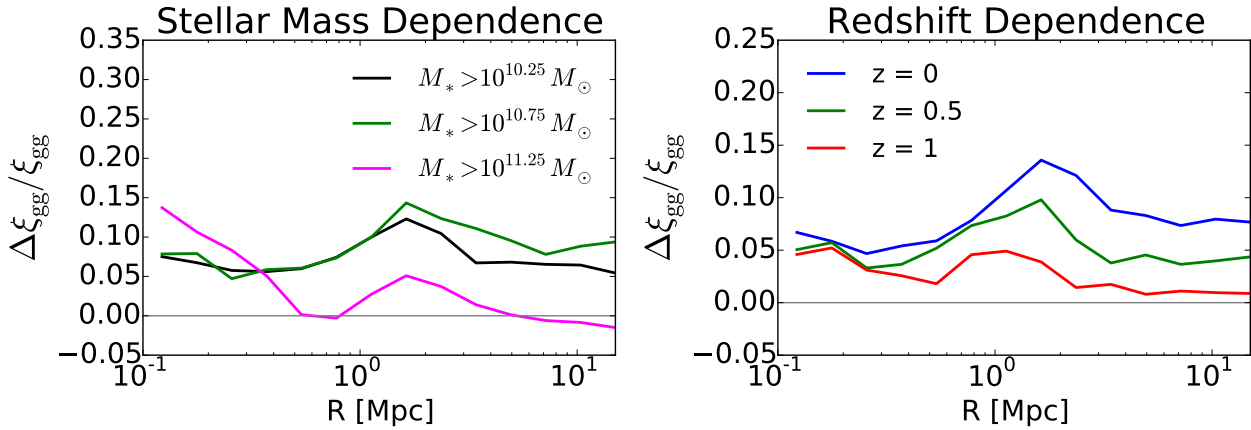


Figure 8. M_* - and z -dependence of assembly bias. All curves in both panels pertain to our fiducial assembly bias model, in which $\mathcal{A}_{\text{bias}}^{\text{cen}} = 1$, $\mathcal{A}_{\text{bias}}^{\text{sat}} = 0.2$, the secondary halo property is concentration and $\sigma_{\log M_*} = 0.4$. In the *left panel*, we show the fractional effect on ξ_{gg} for the three different M_* -thresholds indicated in the legend; in our baseline HOD model, the M_* threshold-dependence derives from the $M_* - M_h$ relation (see Eq. [8]). Over this stellar mass range, the impact of assembly bias generally weakens as the M_* threshold increases; the apparent non-monotonic behavior seen by comparing the green and black curves in the left panel is a numerical resolution artifact, as discussed in the text. In the *right panel* we show how a fixed level of assembly bias has an impact on galaxy clustering with a strength that varies with redshift. In our model z -dependence derives from the evolution of the stellar-to-halo-mass relation (see Eq. [7]). For L^* -type galaxy samples defined by a fixed stellar mass (or luminosity) threshold, the impact of assembly bias on galaxy clustering becomes less important at higher redshift, a generic result.

surface brightness profile). By fitting measurements of n -dependent clustering with an HOD decorated according to t_{lmm} , one can statistically test the hypothesis that galaxy morphology is physically connected to major mergers.

(ii) Let $x = \Delta M_{\text{vir}}/\Delta\tau$ be halo mass accretion rate, defined over some timescale τ , and let $\langle f|M_h \rangle$ be some baseline model for the duty cycles of quasars. By fitting such a decorated HOD to the two-point functions of quasar samples and finding the time τ over which the correlation is strongest, it becomes possible to statistically quantify the timescale over which the cosmic supply of fresh gas impacts the quasar duty cycle.

(iii) Let $x = N_c(M_h)$ be the number of central galaxies in a halo (i.e., zero or one), and let $\langle f|M_h \rangle = \langle N_s|M_h \rangle$. This is the variation on the decorated HOD alluded to in §2.2 that allows one to explore intermediate cases between the two extreme assumptions for how $\langle N_c N_s | M_{\text{vir}} \rangle$ is computed in ordinary HOD models.

We conclude this section by noting that the `Halotools` code base already supports all of the above generality. As described in the code documentation <http://halotools.readthedocs.org>, the `HeavisideAssembias` orthogonal mix-in class can be used to decorate *any* one-point function with the step-function style assembly bias employed in the present paper. There is also freedom to explore $\mathcal{A}_{\text{bias}} = \mathcal{A}_{\text{bias}}(M_h)$, as well as M_h -dependence in how the halos are split into sub-populations, i.e., $P_1 = P_1(M_h)$. This level of generality is made possible through the use of a python decorator, from which the decorated HOD derives its name. We will explore many of these interesting avenues for extending the HOD approach in forthcoming papers.

6.2 Previous Formulations

6.2.1 Early HOD-style models

The general approach taken in our work is most closely related to Wechsler et al. (2006). In that paper, the authors considered generalizing the halo model to predict dark matter and/or galaxy clustering given that the clustering of halos is both mass- and density-profile dependent. Our mathematical formulation of the decorated HOD builds naturally upon this early work by introducing the concept of “HOD conservation” into the framework outlined in Section 4.4 of Wechsler et al. (2006).

Another early formulation of assembly-biased HOD-style models appears in Tinker et al. (2008). There the authors introduced a dependence of the first occupation moment of central galaxies $\langle N_c \rangle$ on δ_5 , the number density of dark matter particles smoothed with a spherical tophat window of radius 5 Mpc. In this model, $\langle N_c | M_h; \delta_5 \rangle \neq \langle N_c | M_h \rangle$, and the level at which the equality is violated is controlled by additional parameters. The baseline HOD model explored in Tinker et al. (2008) included a parameter M_{min} , which can intuitively-but-roughly be thought of as the minimum mass required for a halo to host a central galaxy above a given brightness. In Tinker et al. (2008), the authors implemented assembly bias by manually changing the M_{min} parameter in high- and low-density regions such that the overall number density of galaxies is held fixed.

The model presented in Gil-Marín et al. (2011) has much in common with the Tinker et al. (2008) model. In Gil-Marín et al. (2011), the authors partition the dark matter density field into three disjoint categories, *voids*, *filaments* and *nodes*, and allow the values of all the HOD parameters to separately vary in each of these regions.

These early formulations of assembly bias are conceptually quite different from the decorated HOD. For example, altering the value of M_{\min} as a function of large-scale dark matter density introduces an explicit covariance between the HOD parameter M_{\min} and the additional parameters encoding the assembly bias. The advantage of our formulation is that one is free to change the assembly bias parameters $\mathcal{A}_{\text{bias}}$ while fixing *both* the number density \bar{n}_{g} and all parameters of the baseline model. Decorated HODs have the distinct advantage that the new assembly bias parameters are orthogonal to those that describe the standard baseline model.

6.2.2 Abundance matching-style models

Subhalo abundance matching (SHAM; Kravtsov et al. 2004; Vale & Ostriker 2004) is a class of galaxy-halo models that differs from HOD-style models in several respects. In SHAM, functional forms for $\langle N_{\text{c}}|M_{\text{h}} \rangle$ and $\langle N_{\text{s}}|M_{\text{h}} \rangle$ are never explicitly chosen. Instead, there is an assumed monotonic correspondence between stellar mass M_* and some (sub)halo property x . In the absence of scatter between M_* and x , there exists a unique mapping $\langle M_*|x \rangle$ that yields the correct one-point function, which in this example is the stellar mass function $\phi(M_*)$. By associating host halos with central galaxies and subhalos with satellites, for any stellar mass threshold the functions $\langle N_{\text{c}}|M_{\text{h}} \rangle$ and $\langle N_{\text{s}}|M_{\text{h}} \rangle$ are determined by this unique mapping.

In the most quantitatively successful SHAM models, the property x is chosen to be some measure of the subhalo circular velocity V_{max} (e.g., Conroy et al. 2006; Reddick et al. 2012; Hearin et al. 2012). As pointed out in Zentner et al. (2014), this choice results in significant levels of assembly bias in the following sense: $\langle N_{\text{c}}|M_{\text{vir}}, V_{\text{max}} \rangle \neq \langle N_{\text{c}}|M_{\text{vir}} \rangle$ and $\langle N_{\text{s}}|M_{\text{vir}}, V_{\text{max}} \rangle \neq \langle N_{\text{s}}|M_{\text{vir}} \rangle$. In an interesting recent advance of the abundance matching formalism, Lehmann et al. (2015) explored SHAM models in which the subhalo property x varies between M_{vir} and V_{max} via a continuously-valued parameter α . They fit the newly introduced parameter α to SDSS clustering measurements at $z \approx 0$, and their best-fit model significantly prefers “ V_{max} -like” subhalo properties over “pure- M_{vir} ” properties. That is, low-redshift clustering measurements are better described by SHAM-style models in which $\langle N_{\text{s}} \rangle$ and $\langle N_{\text{c}} \rangle$ do not depend on virial mass M_{vir} alone (see also Mao et al. 2015, for closely related work).

The model presented in this paper implements assembly bias in a very different manner from these and other SHAM-style models of volume-limited galaxy samples. First of all, there are the usual differences between traditional SHAM and HOD implementations: the use of subhalos vs. analytical descriptions of the spatial distribution of satellite galaxies, the explicit vs. implicit parameterization of the occupation moments, etc. Beyond these differences, the above SHAM-style models depend exclusively on a *single* halo property at a time, whereas the decorated HOD permits exploration of the galaxy-halo connection upon two (or more) halo properties simultaneously. Of equal importance, the decorated HOD

provides fully independent control over the level of assembly bias and the “ M_{vir} -only” occupation moments. By contrast, there is no such freedom in SHAM. As a specific example, in the Lehmann et al. (2015) model, the level of assembly bias in $\langle N_{\text{c}} \rangle$ is controlled by the α parameter, but varying this parameter *also* changes the M_{vir} -dependence of the satellite fraction.

6.2.3 Models of galaxy color

The “age-matching” model introduced in Hearin & Watson (2013) makes predictions for the color dependence of the galaxy-halo connection. Age matching is a particular implementation of a class of models called *conditional abundance matching* (CAM, Hearin et al. 2013). As described in §6.2.2, abundance matching models use the one-point function $\phi(M_*)$ as an input that determines the mapping $\langle M_*|x \rangle$ between M_* and some halo property x . Analogously, conditional abundance matching models use the conditional one-point functions $\phi(g-r|M_*)$ to determine the continuously varying probability distribution $P(g-r|x, y)$ of $g-r$ colors as a function of two subhalo properties x and y . These models are formulated such that at fixed values of the primary halo property x , the galaxy property $g-r$ and the subhalo property y are in monotonic correspondence. Motivated by Wechsler et al. (2002) and Bullock et al. (2001), the age matching implementations of CAM that have been most successful (Hearin & Watson 2013; Hearin et al. 2013; Watson et al. 2015; Yamamoto et al. 2015; Saito et al. 2015) choose the primary halo property $x = V_{\text{peak}}$ and the secondary halo property $y = z_{\text{starve}}$, a proxy for the age of the halo (see also Masaki et al. 2013; Kulier & Ostriker 2015).

CAM models can be thought of as one way to generalize the decorated HOD framework to a continuously variable galaxy property. As shown in Campbell et al. (2015, in prep), the strength of the correlation between, for example, $g-r$ and z_{starve} can be smoothly varied, with age matching representing the extreme, maximum correlation strength. In such variations, the conditional one-point functions are held exactly fixed in an analogous fashion to how the first moments of decorated HOD models are held fixed as the $\mathcal{A}_{\text{bias}}$ parameter is varied.

The model presented in Paranjape et al. (2015) is another example of an HOD-style model implementing assembly bias. In the color dependence of this model, one first specifies a model for the red fraction of galaxies (separately for centrals and satellites, as in Skibba & Sheth 2009). Around this baseline model, the red fraction varies according to halo concentration in such a way that the overall red fraction is held fixed. Intriguingly, Paranjape et al. (2015) find that their models prefer relatively strong correlations between the red fraction and halo concentration when comparing to SDSS measurements of “1-halo conformity”: the tendency for red satellites to reside in groups with a red central at fixed group mass.

The Paranjape et al. (2015) model is HOD-conserving and is therefore an example of a decorated HOD model. As described in Paranjape et al. (2015), this generalization of the HOD offers a promising means to understand recent measurements of the galactic con-

formity signal (see Kauffmann et al. 2013; Hearin et al. 2014, 2015; Kavinwanichakij et al. 2015, and references therein for further details).

6.3 Significance for Cosmology

In addition to galaxy formation, the effects of assembly bias can have important consequences for cosmology. HOD-style models are often employed to model the galaxy–dark matter connection in studies that aim to use relatively small-scale galaxy clustering and lensing statistics to constrain cosmological parameters (e.g. Tinker et al. 2005; van den Bosch et al. 2007; Cacciato et al. 2009; Leauthaud et al. 2012; Cacciato et al. 2013; Mandelbaum et al. 2013; More et al. 2013; Villaescusa-Navarro et al. 2014; More et al. 2015). These methods assume that assembly bias is either not present in the observed universe or that it is present only at levels that do not hinder cosmological parameter inference. As assembly bias can compromise the inferred galaxy–dark matter connection (Zentner et al. 2014), it may also induce systematic errors in inferred cosmological parameters and impair tests of general relativity (Hearin 2015). The degree to which such effects may threaten the program of using galaxy clustering on quasilinear and nonlinear scales to constrain cosmology has not yet been quantified. We are actively pursuing this line of research.

In this work, we have studied a new class of models that may be used to incorporate assembly bias into HOD-style analyses of galaxy clustering and lensing statistics. Utilizing these models in cosmological analyses will render any inferred parameters more robust against systematic errors induced by assembly bias. However, the new parameters of assembly bias models may be degenerate with cosmological parameters, and to the degree to which they are degenerate this will degrade the statistical constraints on inferred cosmological parameters. Assessing the degeneracy between cosmological parameters and models of assembly bias is another subject of our ongoing collaborative work.

7 SUMMARY

We conclude the paper with a summary of our primary findings.

(i) We introduce the *decorated HOD*, a new class of models for the galaxy-halo connection designed to account for assembly bias.

(ii) Using a simple two-population decorated HOD, we exhaustively enumerate the litany of signatures that assembly bias imprints on the clustering and lensing of M_* –threshold galaxy samples. For the clustering of SDSS Main Galaxy Sample-type galaxies, the effects can be as large as a factor of two on 200 kpc scales, and up to $\sim 15\%$ in the linear regime. For lensing, the effects are limited to the $\sim 10 - 15\%$ level on all scales.

(iii) For galaxy samples selected by a fixed stellar mass threshold, the impact of assembly bias on clustering and lensing generally weakens with redshift.

(iv) The scale dependence of assembly bias is complex. We advocate that flexible analysis techniques such as those provided by the open-source **Halotools** package will be necessary in order for the precision-cosmology program to proceed into the quasilinear and nonlinear regime.

We refer readers to the repository stored at <https://github.com/aphearin/decorated-hod-paper>, which contains an annotated IPython Notebook that can be used to reproduce our figures, as well as a frozen copy of the exact version of the **Halotools** code base we used to generate our results.

ACKNOWLEDGMENTS

The work of ARZ was funded by the U.S. National Science Foundation under grant AST 1517563 and by the Pittsburgh Particle physics, Astrophysics, and Cosmology Center (Pitt PACC) at the University of Pittsburgh. The work of FvdB was funded by the U.S. National Science Foundation under grant AST 1516962. A portion of this work was also supported by the National Science Foundation under grant PHYS-1066293 and the hospitality of the Aspen Center for Physics. Support for EJT was provided by NASA through Hubble Fellowship grants #51316.01 awarded by the Space Telescope Science Institute, which is operated by the Association of Universities for Research in Astronomy, Inc., for NASA, under contract NAS 5-26555. APH is funded by the Yale Center for Astronomy & Astrophysics, and thanks Doug Watson for useful comments and Link Wray for the generous, sublime boogie of *I’m So Glad, I’m So Proud*.

REFERENCES

- Adhikari S., Dalal N., Chamberlain R. T., 2014, JCAP, 11, 19
- Astropy Collaboration Robitaille T. P., Tollerud E. J., Greenfield P., Droettboom M., Bray E., Aldcroft T., et al., 2013, AAP, 558, A33
- Behnel S., Bradshaw R., Citro C., Dalcin L., Seljebotn D., Smith K., 2011, Computing in Science Engineering, 13, 31
- Behroozi P. S., Conroy C., Wechsler R. H., 2010, ApJ, 717, 379
- Behroozi P. S., Wechsler R. H., Conroy C., 2013, ApJ, 770, 57
- Behroozi P. S., Wechsler R. H., Wu H.-Y., 2011, ArXiv:1110.4372
- Behroozi P. S., Wechsler R. H., Wu H.-Y., Busha M. T., Klypin A. A., Primack J. R., 2013, ApJ, 763, 18
- Berlind A. A., Weinberg D. H., 2002, ApJ, 575, 587
- Blanton M. R., Berlind A. A., 2007, ApJ, 664, 791
- Blanton M. R., Eisenstein D., Hogg D. W., Zehavi I., 2006, ApJ, 645, 977
- Bray A. D., et al., 2016, MNRAS, 455, 185
- Bullock J. S., Kolatt T. S., Sigad Y., Somerville R. S., Kravtsov A. V., Klypin A. A., Primack J. R., Dekel A., 2001, MNRAS, 321, 559

- Cacciato M., van den Bosch F. C., More S., Li R., Mo H. J., Yang X., 2009, *MNRAS* , 394, 929
- Cacciato M., van den Bosch F. C., More S., Mo H., Yang X., 2013, *MNRAS* , 430, 767
- Collister A. A., Lahav O., 2005, *MNRAS* , 361, 415
- Conroy C., Wechsler R. H., 2009, *ApJ* , 696, 620
- Conroy C., Wechsler R. H., Kravtsov A. V., 2006, *ApJ* , 647, 201
- Cooray A., Sheth R., 2002, *Phys. Rep.* , 372, 1
- Croton D. J., Gao L., White S. D. M., 2007, *MNRAS* , 374, 1303
- Dalal N., White M., Bond J. R., Shirokov A., 2008, *ApJ* , 687, 12
- Diemer B., Kravtsov A. V., 2014, *ApJ* , 789, 1
- Feldmann R., Mayer L., 2015, *MNRAS* , 446, 1939
- Gao L., Springel V., White S. D. M., 2005, *MNRAS* , 363, L66
- Gao L., White S. D. M., 2007, *MNRAS* , 377, L5
- Gil-Marín H., Jimenez R., Verde L., 2011, *MNRAS* , 414, 1207
- Gottloeber S., Klypin A., 2008, *ArXiv:0803.4343*
- Guo H., Zheng Z., Zehavi I., Xu H., Eisenstein D. J., Weinberg D. H., Bahcall N. A., Berlind A. A., Comparat J., McBride C. K., Ross A. J., Schneider D. P., Skibba R. A., Swanson M. E. C., Tinker J. L., Tojeiro R., Wake D. A., 2014, *ArXiv:1401.3009*
- Guo Q., White S., Boylan-Kolchin M., De Lucia G., Kauffmann G., Lemson G., Li C., Springel V., Weinmann S., 2011, *MNRAS* , 413, 101
- Hearin A. P., 2015, *MNRAS* , 451, L45
- Hearin A. P., Behroozi P. S., van den Bosch F. C., 2015, *ArXiv:1504.05578*
- Hearin A. P., Watson D. F., 2013, *ArXiv:1304.5557*
- Hearin A. P., Watson D. F., Becker M. R., Reyes R., Berlind A. A., Zentner A. R., 2013, *ArXiv:1310.6747*
- Hearin A. P., Watson D. F., van den Bosch F. C., 2014, *ArXiv:1404.6524*
- Hearin A. P., Zentner A. R., Berlind A. A., Newman J. A., 2012, *ArXiv:1210.4927*
- Heitmann K., Higdon D., White M., Habib S., Williams B. J., Lawrence E., Wagner C., 2009, *ApJ* , 705, 156
- Heitmann K., White M., Wagner C., Habib S., Higdon D., 2010, *ApJ* , 715, 104
- Jiang F., van den Bosch F. C., 2015, *MNRAS* , 453, 3575
- Kauffmann G., Li C., Zhang W., Weinmann S., 2013, *MNRAS* , 430, 1447
- Kauffmann G., White S. D. M., Heckman T. M., Ménard B., Brinchmann J., Charlot S., Tremonti C., Brinkmann J., 2004, *MNRAS* , 353, 713
- Kawinwanichakij L., et al., 2015, *ArXiv:1511.02862*
- Klypin A. A., Trujillo-Gomez S., Primack J., 2011, *ApJ* , 740, 102
- Kravtsov A. V., Berlind A. A., Wechsler R. H., Klypin A. A., Gottlöber S., Allgood B., Primack J. R., 2004, *ApJ* , 609, 35
- Kravtsov A. V., Klypin A. A., Khokhlov A. M., 1997, *ApJS* , 111, 73
- Kulier A., Ostriker J. P., 2015, *MNRAS* , 452, 4013
- Lacerna I., Padilla N., 2011, *MNRAS* , 412, 1283
- Landy S. D., Szalay A. S., 1993, *ApJ* , 412, 64
- Leauthaud A., et al., 2011, *ArXiv:1104.0928*
- Leauthaud A., et al., 2012, *ApJ* , 744, 159
- Leauthaud A., Tinker J., Behroozi P. S., Busha M. T., Wechsler R. H., 2011, *ApJ* , 738, 45
- Lehmann B. V., Mao Y.-Y., Becker M. R., Skillman S. W., Wechsler R. H., 2015, *ArXiv:1510.05651*
- Lin Y.-T., Mandelbaum R., Huang Y.-H., Huang H.-J., Dalal N., Diemer B., Jian H.-Y., Kravtsov A., 2015, *ArXiv:1504.07632*
- Ma C.-P., Fry J. N., 2000, *ApJ* , 543, 503
- Mandelbaum R., et al., 2005, *MNRAS* , 361, 1287
- Mandelbaum R., Slosar A., Baldauf T., Seljak U., Hirata C. M., Nakajima R., Reyes R., Smith R. E., 2013, *MNRAS* , 432, 1544
- Mao Y.-Y., Williamson M., Wechsler R. H., 2015, *ApJ* , 810, 21
- Masaki S., Lin Y.-T., Yoshida N., 2013, *ArXiv:1301.1217*
- Miyatake H., More S., Takada M., Spergel D. N., Mandelbaum R., Rykoff E. S., Rozo E., 2015, *ArXiv:1506.06135*
- Mo H., van den Bosch F. C., White S., 2010, *Galaxy Formation and Evolution*. Cambridge University Press, Cambridge, UK
- Mo H. J., Yang X., van den Bosch F. C., Jing Y. P., 2004, *MNRAS* , 349, 205
- More S., Diemer B., Kravtsov A. V., 2015, *ApJ* , 810, 36
- More S., van den Bosch F. C., Cacciato M., More A., Mo H., Yang X., 2013, *MNRAS* , 430, 747
- Moster B. P., Naab T., White S. D. M., 2013, *MNRAS* , 428, 3121
- Navarro J. F., Frenk C. S., White S. D. M., 1997, *ApJ* , 490, 493
- Paranjape A., Kovač K., Hartley W. G., Pahwa I., 2015, *MNRAS* , 454, 3030
- Porciani C., Magliocchetti M., Norberg P., 2004, *MNRAS* , 355, 1010
- Porciani C., Norberg P., 2006, *MNRAS* , 371, 1824
- Purcell C. W., Bullock J. S., Zentner A. R., 2007, *ApJ* , 666, 20
- Reddick R. M., Wechsler R. H., Tinker J. L., Behroozi P. S., 2012, *ArXiv:1207.2160*
- Reid B. A., Seo H.-J., Leauthaud A., Tinker J. L., White M., 2014, *MNRAS* , 444, 476
- Riebe K., Partl A. M., Enke H., Forero-Romero J., Gottloeber S., Klypin A., Lemson G., Prada F., Primack J. R., Steinmetz M., Turchaninov V., 2011, *ArXiv:1109.0003*
- Rodriguez-Puebla A., Avila-Reese V., Firmani C., Colin P., 2011, *ArXiv:1103.4151*
- Ross A. J., Brunner R. J., 2009, *MNRAS* , 399, 878
- Saito S., Leauthaud A., Hearin A. P., Bundy K., Zentner A. R., Behroozi P. S., Reid B. A., Sinha M., Coupon J., Tinker J. L., White M., Schneider D. P., 2015, *ArXiv:1509.00482*
- Scoccimarro R., Sheth R. K., Hui L., Jain B., 2001, *ApJ* , 546, 20
- Seljak U., 2000, *MNRAS* , 318, 203
- Seljak U., Makarov A., Mandelbaum R., Hirata C. M., Padmanabhan N., McDonald P., Blanton M. R., Tegmark M., Bahcall N. A., Brinkmann J., 2005, *PRD* , 71, 043511
- Skibba R. A., Sheth R. K., 2009, *MNRAS* , 392, 1080

- Sunayama T., Hearin A. P., Padmanabhan N., Leauthaud A., 2015, ArXiv:1509.06417
- Tinker J., Kravtsov A. V., Klypin A., Abazajian K., Warren M., Yepes G., Gottlöber S., Holz D. E., 2008, ApJ , 688, 709
- Tinker J. L., Conroy C., Norberg P., Patiri S. G., Weinberg D. H., Warren M. S., 2008, ApJ , 686, 53
- Tinker J. L., Leauthaud A., Bundy K., George M. R., Behroozi P., Massey R., Rhodes J., Wechsler R., 2013, ArXiv:1308.2974
- Tinker J. L., Robertson B. E., Kravtsov A. V., Klypin A., Warren M. S., Yepes G., Gottlöber S., 2010, ApJ , 724, 878
- Tinker J. L., Weinberg D. H., Zheng Z., Zehavi I., 2005, ApJ , 631, 41
- Vale A., Ostriker J. P., 2004, MNRAS , 353, 189
- van den Bosch F. C., Mo H. J., Yang X., 2003, MNRAS , 345, 923
- van den Bosch F. C., More S., Cacciato M., Mo H., Yang X., 2013, MNRAS , 430, 725
- van den Bosch F. C., Tormen G., Giocoli C., 2005, MNRAS , 359, 1029
- van den Bosch F. C., Yang X., Mo H. J., 2003, MNRAS , 340, 771
- van den Bosch F. C., Yang X., Mo H. J., Weinmann S. M., Macciò A. V., More S., Cacciato M., Skibba R., Kang X., 2007, MNRAS , 376, 841
- Villaescusa-Navarro F., Marulli F., Viel M., Branchini E., Castorina E., Sefusatti E., Saito S., 2014, J. Cosmol. Astropart. Phys., 3, 11
- Wake D. A., Sheth R. K., Nichol R. C., Baugh C. M., Bland-Hawthorn J., Colless M., Couch W. J., Croom S. M., de Propris R., Drinkwater M. J., Edge A. C., Loveday J., Lam T. Y., Pimbblet K. A., Roseboom I. G., Ross N. P., Schneider D. P., Shanks T., Sharp R. G., 2008, MNRAS , 387, 1045
- Wake D. A., Whitaker K. E., Labbé I., van Dokkum P. G., Franx M., Quadri R., Brammer G., Kriek M., Lundgren B. F., Marchesini D., Muzzin A., 2011, ApJ , 728, 46
- Wang L., Weinmann S. M., De Lucia G., Yang X., 2013, MNRAS , 433, 515
- Wang Y., Yang X., Mo H. J., van den Bosch F. C., Weinmann S. M., Chu Y., 2008, ApJ , 687, 919
- Watson D. F., Berlind A. A., Zentner A. R., 2011, ApJ , 738, 22
- Watson D. F., Hearin A. P., Berlind A. A., Becker M. R., Behroozi P. S., Skibba R. A., Reyes R., Zentner A. R., van den Bosch F. C., 2015, MNRAS , 446, 651
- Wechsler R. H., Bullock J. S., Primack J. R., Kravtsov A. V., Dekel A., 2002, ApJ , 568, 52
- Wechsler R. H., Zentner A. R., Bullock J. S., Kravtsov A. V., Allgood B., 2006, ApJ , 652, 71
- Weinmann S. M., van den Bosch F. C., Yang X., Mo H. J., 2006, MNRAS , 366, 2
- Yamamoto M., Masaki S., Hikage C., 2015, ArXiv:1503.03973
- Yang X., Mo H. J., van den Bosch F. C., 2003, MNRAS , 339, 1057
- Yang X., Mo H. J., van den Bosch F. C., 2006, ApJL , 638, L55
- Yang X., Mo H. J., van den Bosch F. C., 2009a, ApJ , 695, 900
- Yang X., Mo H. J., van den Bosch F. C., 2009b, ApJ , 693, 830
- Yang X., Mo H. J., van den Bosch F. C., Zhang Y., Han J., 2012, ApJ , 752, 41
- Yang X., Mo H. J., Zhang Y., van den Bosch F. C., 2011, ApJ , 741, 13
- Yoo J., Tinker J. L., Weinberg D. H., Zheng Z., Katz N., Davé R., 2006, ApJ , 652, 26
- Zehavi I., et al., 2005, ApJ , 630, 1
- Zehavi I., et al., 2011, ApJ , 736, 59
- Zentner A. R., 2007, International Journal of Modern Physics D, 16, 763
- Zentner A. R., Berlind A. A., Bullock J. S., Kravtsov A. V., Wechsler R. H., 2005, ApJ , 624, 505
- Zentner A. R., Hearin A. P., van den Bosch F. C., 2014, MNRAS , 443, 3044
- Zheng Z., Coil A. L., Zehavi I., 2007, ApJ , 667, 760
- Zhu G., Zheng Z., Lin W. P., Jing Y. P., Kang X., Gao L., 2006, ApJL , 639, L5
- Zu Y., Mandelbaum R., 2015, ArXiv:1509.06758